Optimisation And Adaptable Wave Energy Point Absorber Array Design

Thesis

by

Sung-Hsien Huang

Delft University of Technology

Offshore & Dredging Engineering

Instructor:	George Lavidas
Supervisor:	Vaibhav Raghavan
Project Duration:	1 November, 2023 - 10 October, 2024
Faculty:	Faculty of Civil Engineering and Geosciences

TU Delft

Abstract

Array design of a wave farm composed of multiple WECs is an essential issue during the design phase of an offshore wave energy farm. Although various research has looked into the optimal array design, the optimization process usually takes a lot of time.

The objective of this thesis is to reduce the time required during the WEC design phase. The study focuses on performing a hydrodynamic analysis of a wave farm consisting of four single-point absorbers, examining the relationship between excitation force and array spacing, and determining the average total power production of the wave farm.

This thesis employs the Boundary Element Method (BEM) to analyze the hydrodynamic interactions of waves and oscillatory motions in WECs. Using the open-source software Capytaine, it estimates key hydrodynamic coefficients and solves the system of equations via Green's theorem to evaluate added mass and excitation forces. By selecting excitation force as a design parameter, a linear regression model is established. Furthermore, a machine learning model based on the Random Forest algorithm is developed to capture the complex relationship between total power output and the design parameter. After the machine learning model is created, the optimal array spacing for a specific site can be estimated quickly by combining results with a wave scatter diagram.

These findings aim to contribute to wave energy systems design by providing a reliable link between hydrodynamic results and design parameters and accelerating development in the wave energy sector.

Contents

List of Figures

List of Tables

Nomenclature

Abbreviations

Abbreviation	Definition
BEM	Boundary Element Method
CAD	Computer-Aided Design
CFD	Computational Fluid Dynamics
CNN	Convolutional Neural Networ
EA	Evolution Algorithm
GA	Genetic Algorithm
HCCA	Hybrid Cooperative Co-evolution Algorithm
ISA	International Standard Atmosphere
MCM	Monte Carlo Method
MLP	Multi-Layer Perceptron
ML	Machine Learning
MSE	Mean Square Error
OBUIE	Observed-Based Unknown Input Estimator
OWC	Oscillating Water Column
PA	Point Absorber
PSO	Particle Swarm
PTO	Power take-off
RAO	Response Amplitude Operator
RBF	Radial Basis Functions
WEC	Wave Energy Converter

Symbols

Symbol	Definition	Unit
h	Water depth	[m]
V	Velocity	[m/s]
k	Wave number	[rad/m]
p	Pressure	[N/m^2]
n	Normal vector	[-]
a_{ij}	Added mass coefficient	[kg]
b_{ij}	Radiation damping coefficient	[kg/s]
c_{ij}	Restoring coefficient	[N/m]
x_b	x component of buoyancy center	[-]

Symbol	Definition	Unit
y_b	y component of buoyancy center	[-]
z_b	z component of buoyancy center	[-]
x_g	x component of gravitational center	[-]
y_g	y component of gravitational center	[-]
z_g	z component of gravitational center	[-]
Z_i	Intrisic impedance	[kg/ms]
ρ	Water density	[kg/m^3]
β	Wave direction	[-]
ζ	Wave amplitude	[m]
$\hat{\zeta}$	Complex amplitude of body motion	[m]
$\hat{\zeta}_a$	Complex amplitude of wave	[m]
$\hat{\zeta}_j$	Complex amplitude of body motion in i degree of freedom	[m]
Φ	Velocity potential time domain	[m^2/s]
Φ_r	Radiation potential	[m^2/s]
Φ_0	Incoming wave potential	[m^2/s]
Φ_7	Scattered wave potential	[m^2/s]
ϕ	Potential in frequency domain	[m^2]
ϕ_0	Incoming wave potential	[m^2]
η	Free surface elevation	[m]
ω	Wave frequency	[rad/s]

1

Introduction

1.1. Background

In 1973, a disruption in crude oil supplies led to a significant shift in energy policy [1]. During this period, the increasing oil prices caused a growing interest in wave energy production. Numerous research and conferences supported by the British and Norwegian governments began to explore the potential of wave energy. In 1991, the European Commission decided to include wave energy in its renewable energy plans, and sponsor various wave energy projects [2]. Nowadays, the European Union continues to invest in these projects, aiming to increase the installed wave energy capacity to 40GW by 2050 [3].

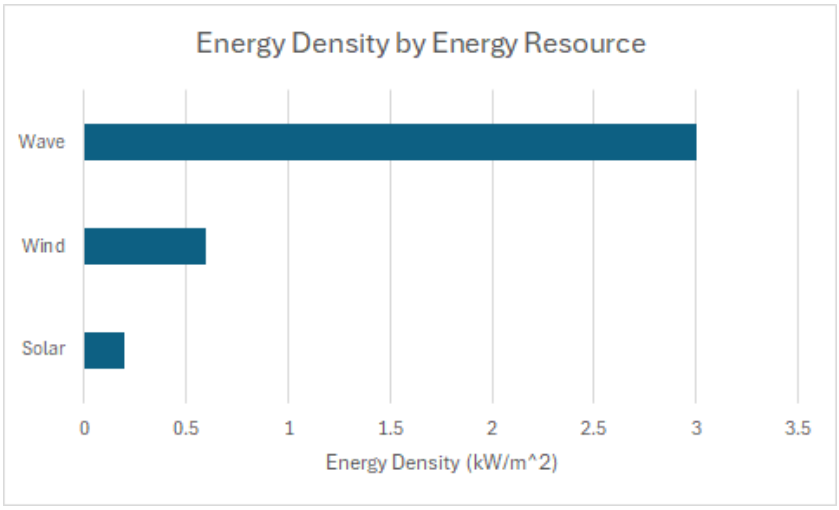

Figure 1.1: Energy Density Comparison (Data compiled from Iván A. Hernández-Robles et al. [4])

Wave energy is regarded as one of the highest energy-dense and predictable offshore renewable energy [5][4]. The key advantage of wave energy is its predictability, which makes the electricity grid more stable [6]. Due to the higher density of water, the scale size of the wave energy converter can be much smaller when compared to

a wind turbine, meaning a saving in material [7]. Additionally, wave energy offers high flexibility which allows WECs to operate at various sites or be integrated with other offshore structures. It can be utilized for powering marine buoys, lighthouses, and large-scale power generation, with minimal regional limitations[8].

To sum up, wave energy stands out as a reliable and highly promising renewable energy source. To reach the target of net-zero greenhouse gas emissions by 2050, integrating wave energy into future energy plans is crucial.

1.2. Wave Energy Converter Overview

A wave energy converter (WEC) is a device designed to capture energy from ocean waves and transform it into electricity or another form of usable power. WECs can be classified into various types based on their underlying principles for converting wave oscillations into electricity.

1.2.1. Oscillating Water Column

An oscillating water column (OWC) is a device that transforms airflow within a chamber and converts it into electricity. It is a type of WEC that operates based on the rise and fall of water within a chamber caused by the oscillating motion of waves [9][10][11]. The structure typically consists of a hollow chamber partially submerged in the water, with an open bottom facing the ocean and a sealed top. As waves move in, the water level within the chamber increases, compressing the air trapped above. This compressed air goes through a turbine, which drives a generator to produce electricity. There are two types of OWC: fixed and floating type. The advantage of fixed OWC is the high reliability because it has no moving parts in the water, making it easier to maintain. On the other hand, floating OWCs have the advantage of reduced noise because they are located farther from the shoreline.

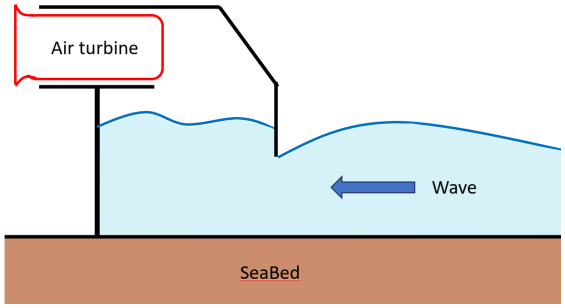

Figure 1.2: Fixed oscillating water column structure

1.2.2. Point Absorber

A point absorber (PA) is a floating device that reacts to wave motion by moving vertically or horizontally. It usually includes a buoyant structure and a power take-off (PTO) system. Different configurations of these components lead to various types of point absorbers. In a one-body heave design, the buoy is connected to a fixed structure on the seabed by a cable and a spring mechanism. This arrangement allows the

PTO system to engage based on the relative motion between the floating part on the surface and the submerged part.

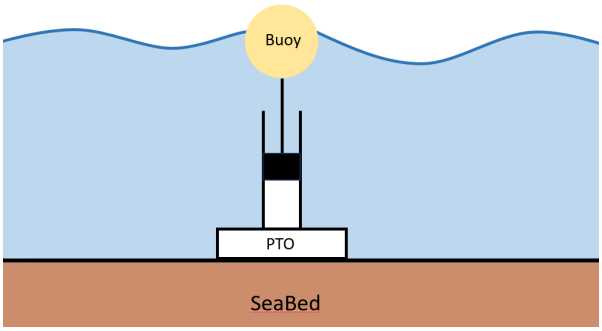

Figure 1.3: Schematic drawing of point absorber

1.2.3. Attenuator

Attenuators are long, floating structures consisting of multiple floating bodies connected by hinged joints that align perpendicular to the direction of the waves. The energy is generated from the relative rotation between the adjacent segments. This movement creates mechanical energy, which is then converted into electrical power using different mechanisms, such as linear generators.

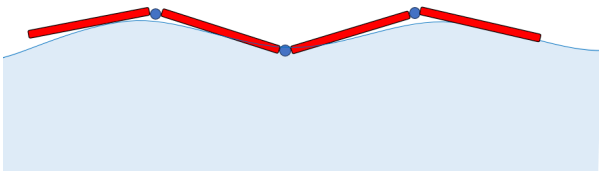

Figure 1.4: Schematic drawing of attenuator

1.3. Research Gap

1. Finding the relation between design parameters and excitation forces within a wave farm

Determining the excitation forces experienced by a WEC experience is essential for evaluating its lifetime. Deriving excitation forces without performing hydrodynamic analysis is not possible, and the process becomes time-consuming as design parameters increase. However, limited research has focused on establishing an approximate mathematical relationship between excitation forces and other parameters. Once this relationship is identified, deriving excitation forces will become more straightforward, which can significantly reduce the required time to assess the lifetime of the WEC.

2. Finding a way to estimate power production in a short time

Most of the research that has been proposed used numerical comparison methods to achieve optimization considering power production and array configuration. Recently, there has been an emergence of research using artificial intelligence methods. However, these methods usually require a huge amount of time to analyze, and the result is only suitable for individual cases. Thus, a research gap exists with the goal of reducing calculation time. One of the objectives of this research is to find out the mathematical relation between array configuration factors and the final power production. Once the models are trained, a broader range of cases can be investigated in a shorter time.

3. Optimization of Array Design and Power Production

Most previous research focuses on predicting power output from a single device. However, wave farms typically contain multiple devices with various array configurations. These configurations should also be considered in power prediction analysis. In this thesis, a square array design consisting of four devices is used, and the spacing between devices is also included as a crucial parameter in the power analysis. By doing so, the overall power production of the wave farm can be more accurately predicted.

1.4. Research Objective

1. Find an effective way to estimate excitation forces and power production

A mathematical formulation is used to estimate the excitation forces, while a machine learning model is utilized to predict power production. After running several cases with different array designs, a mathematical relationship between excitation forces and wave frequency will be established. Following this, multiple hydrodynamic analyses will be conducted, and the resulting data will be used to train a ML model for power estimation.

2. Perform optimization and predict power production

The final goal of this research is to discover an optimal solution for the WEC array layout. With a trained machine learning model, the predicted power production in any given sea state can be easily estimated.

1.5. Outline of The Thesis

In chapter 2 research on previous literature is performed. A comparison between available methods is conducted, and various similar questions proposed before are discussed. chapter 3 elaborates on the background theory of BEM software used in this thesis and explain the derivation process of power production. chapter 4 outlines the overall methodology used in this thesis to address the research question. chapter 5 shows the whole process of solving the hydrodynamic problems for multiple devices in Capytaine. After performing hydrodynamic analysis, chapter 6 presents the

derivation process and the result of the mathematical relation between the excitation forces and design parameters. In chapter 7 the data generated in the previous step are used to train the machine learning model. Once the model is trained the optimal array spacing between 2 devices in a square-shaped wave farm can be determined. Finally, chapter 8 summarizes the overall result and identifies the limitations of the findings.

1.6. Highlight

1. Setting up the relationship between forces and array layout

Although the leading method to estimate the excitation forces on a floating body is using the machine learning method, an effort is made in this thesis to set up the mathematical relationship between the forces and design parameters. After derivation, an evaluation is made to check the reliability of this formulation.

2. Perform hydrodynamic analysis of multi-body in Capytaine

Capytaine does not really support multi-body fluid interaction due to the way it processes input data. However, for hydrodynamic problems, a multi-body system with 6 DOFs can be effectively treated as a single body with generalized DOFs [12], making the hydrodynamic analysis feasible. While limited literature has explored multi-body hydrodynamic analysis using Capytaine, this thesis offers a deeper understanding of the application in this context.

2

Literature Review

Before addressing the optimization problem of the WEC array, a comprehensive literature review was conducted. The main objective of this study is to enhance the breadth of knowledge and to get deeper insight into the array design of the wave farm. By examining existing studies and available methods, the methodology used to address the research questions can be determined.

2.1. Numerical Method Overview

Thanks to the highly developed computer technology, numerical methods are capable of solving hydrodynamic problems, and this relies on the application of the Boundary Element Method (BEM). In the frequency domain, BEM is used to solve Green's functions on the wetted surface of a floating body. For time-domain problems, the Cummins Equation and Computational Fluid Dynamics (CFD) are the primary approaches used to capture nonlinearities that cannot be addressed in the frequency domain.

2.1.1. Frequency Domain Model

The hydrodynamic problem can be modeled using a simplified linear approach, where wave amplitude is relatively small compared to the wavelength. Additionally, when reactive forces like moorings and PTO (with a linear damper) are represented linearly, the dynamics of WECs can be described using linear equations. It also means that the superposition principle holds [13]. Consequently, the dynamics of WECs can be analyzed effectively in the frequency domain because all the non-linearity terms are ignored. In this context, the equations of motion transform into a system of linear equations that can be solved directly.

To evaluate the radiation and excitation loads on the device, the Boundary Element Method (BEM) is employed. Newman[14] developed approximations of the free-surface Green function applicable across all frequency ranges and water depths. This advancement facilitates the analysis of hydrodynamics for complex offshore structures. The approach uses Green's theorem [15] to calculate all the hydrodynamic coefficients, such as added mass and radiation damping, and hydrodynamic forces.

Green's theorem is the application of the Green functions which enable the velocity potential over the submerged part of the body to satisfy the required boundary conditions [16][17]. By solving these integral equations, one can determine the added mass, radiation damping, and excitation forces.

Commonly used frequency-domain models, such as NEMOH, Capytaine, Ansys-AQWA, and WAMIT, are all based on potential flow theory. NEMOH and Capytaine are open-source BEM solvers, with NEMOH developed in Fortran programming language and Capytaine being a Python package rewritten from NEMOH. These tools are designed to calculate first-order hydrodynamic coefficients and excitation forces. In contrast, Ansys-AQWA and WAMIT are commercial software capable of handling second-order nonlinear behaviors.

2.1.2. Time Domain Model

Time-domain models can effectively handle nonlinearities resulting from various components within the energy chain. They also allow for more complex formulations of fluid interactions, which lead to nonlinear hydrodynamic forces. A time-domain model is generally unavoidable in the PTO configurations applied on the WECs due to the complex systems involved [18][19]. Furthermore, when validating a solution based on real sea-state performance, a time-domain model becomes necessary [15]. The time domain approach involves calculating the dynamics of floating bodies directly over time. Typical methods within this framework include the application of Cummins Equation [20] in Potential Flow Theory and Computational Fluid Dynamics (CFD).

Application of Cummins Equation relies on the application of potential flow theory discussed in section 3.2. This approach uses Cummins equations to address hydrodynamic problems through a system of differential equations. By importing hydrodynamic coefficients from frequency-domain solvers, such as Capytaine, the Cummins Equation is then used to determine the motion and forces in the time domain.

Computational Fluid Dynamics (CFD) is a numerical technique used to solve the governing Navier-Stokes equations related to fluid flows. Apart from its wide application in the aerospace sector, CFD is also valuable in the study of wave energy. Specifically, it can predict the performance of WECs in extreme sea conditions, where assumptions required for potential flow theory like small wave steepness are no longer valid.

Notable time-domain numerical software includes OpenFOAM, WEC-Sim, and FLOW-3D. OpenFOAM is an open-source CFD software based on the finite volume method. It solves the governing Navier-Stokes equations on the discrete control volume. WEC-Sim is another free solver for the simulation of WECs. It reads the hydrodynamic coefficients from other frequency-domain solvers and solves Cummins Equation [21] to determine the motion and forces. FLOW-3D is a commercial CFD software that uses finite volume method to solve the Navier-Stokes equations for fluid flow [22]. In an analysis performed by Mohammad[23], a new kind of WEC was examined through experimental research and numerical simulation using FLOW-3D. By comparing the results between the two methods, FLOW-3D showed a good agreement.

Table 2.1: Summary of 3 Different Open-Source Numerical Tools

	Capytaine	OpenFOAM	WEC-Sim
Analysis Domain	Frequency domain	Time domain	Time domain
Fundamental Principle	Potential Flow Theory	Computational Fluid Dynamics	Potential Flow Theory and Cummin Equations
Programming Language	Python	C++	MATLAB
Limitation	Relatively new software that requires more validation	Long calculation time	Does not model highly nonlinear hydrodynamic events such as wave slamming[24]

2.2. Optimization Method Overview

In order to evaluate the effectiveness of optimizing WEC arrays, specific parameters need to be considered. One such parameter is the q factor, which is proportional to the total output power of the entire array and is defined as:

$$q = \frac{P_{total}}{N \cdot P_{isolated}} \tag{2.1}$$

In Equation 2.1, P_{total} is the total power generated by the WEC farm combined with multiple WECs, N is the number of WECs, and $P_{isolated}$ is the power generated by a single WEC. Research[25] has shown that q-factor can be greater than 1 in theory.

When q is less than 1, the average power per WEC in the overall wave farm is lower than that of an isolated WEC. Conversely, if q is greater than 1, the location of the WEC are in the optimal layout and result in a better performance.

There are many methods dealing with the optimization problems of WEC array. For example: Genetic Algorithm (GA) and Monte Carlo Method (MCM)[26].

GA is an algorithm used for finding the optimal solution. The term ”genetic” indicates that the core idea of the algorithm is based on natural selection, which is the process that drives biological evolution [27]. The algorithm starts with a population of individuals, where each individual represents a potential solution to the problem. GA continuously generates a large number of individual solutions. In each iteration, the algorithm selects individuals as parents and uses them to create the next generation of solutions.

The Monte Carlo Method (MLM) solves optimization problems through random sampling. Initially, a large number of samples are generated with randomly selected design parameters such as water depth and array spacing. The resulting q factor is then calculated for each sample, and the optimal design is identified as the one that yields the maximum q factor.

2.3. Review on Machine Learning Method

Machine learning (ML) is a method that enables machines to process and analyze data efficiently[28]. It is particularly effective at extracting valuable insights from large datasets. ML utilizes various algorithms to handle data-related problems. For the optimization problem of the WEC array, the Random Forest Regressor and Neural Network are two of the most commonly used algorithms.

2.3.1. Random Forest Regressor

Random Forest Regressor is one of the algorithms of the machine learning method. The fundamental concept of the algorithm is the formation of decision trees. A decision tree recursively divides the original dataset by creating decision nodes. A decision node contains the condition of how the data would be split and classified into the next nodes. At the end of the decision nodes are the leaf nodes, and they store the prediction of the target variable. The term ”random forest” is an ensemble used to describe the randomly selected decision trees. Each tree is trained on a different random subset of the data. These randomly selected trees help decrease the sensitivity of the model to the variance of the initial data, leading to better generalization and improved performance on unseen data[29]. At each node of the tree, a random subset of features is selected to further decrease correlation among each tree. Afterward, the potential split points are evaluated. The algorithm chooses the split that minimizes the impurity in the resulting child nodes. Impurity is typically measured by metrics like Mean Squared Error (MSE) for regression tasks. Finally, The process of finding the best split is repeated recursively for each child node, and the predictions are made by averaging the outputs of all the trees in the forest.

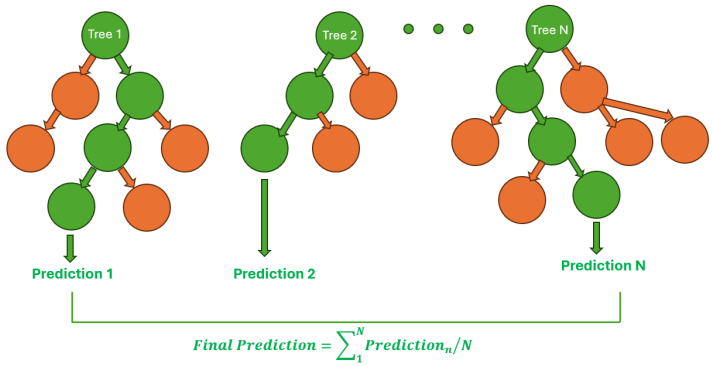

Figure 2.1: Random Forest Schematic Diagram

2.3.2. Neural Network

The term ”Neural Network” refers to a broad category of models inspired by the human brain’s network of neurons. This category covers various architectures and models designed for different tasks. The fundamental component of a neural network is the neuron. A neuron receives one or more inputs, processes them by calculating a weighted sum, adds a bias, and then applies an activation function to generate an output. Neural Networks come in various types based on the geometric architecture

of their neurons. The most common types used in data analysis include Multi-layer Perceptrons (MLPs) and Radial Basic Functions (RBF)

Multi-Layer Perceptron

The architecture of the MLP method is made up of multiple neurons organized into layers, typically comprising an input layer, several hidden layers, and an output layer. During training, the input data moves sequentially through each layer of the network. Each neuron within a layer has its own set of weights and biases. The weights modify the impact of each input feature, while the bias enables the activation function to shift, influencing whether the neuron is activated. The output of each neuron is calculated and sent to the subsequent layer until the final result is obtained. A diagram of MLP is shown in Figure 2.2

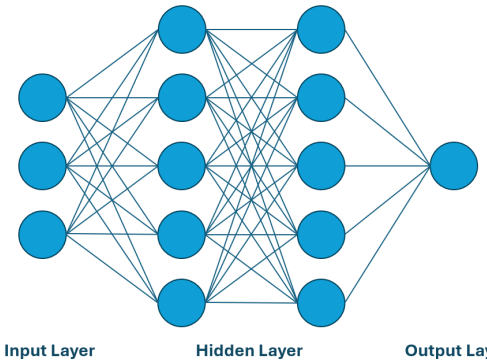

Figure 2.2: Multi-Layer Perceptron Schematic Diagram

Radial Basis Functions

Unlike the MLP method which usually has multiple hidden layers, the RBF method consists of only one hidden layer, along with a single input layer and a single output layer. This method uses radial basis functions ϕ as activation functions to form the neurons in the hidden layer. These functions depend on the distance between the input and certain center points, which enables the network to model complex, non-linear relationships effectively. A schematic drawing of RBF is shown in Figure 2.3

2.4. Review on Load Estimation

The accurate estimation of WEC loads is crucial in the design process of an offshore wave farm. By setting up a precise relation between the loads and other parameters, one can fasten the design cycle and optimization process of the wave farm.

Various research has investigated the estimation of forces on the WEC. Krishna Kumar[30] collected characteristic wave data in different sites and estimated sea state characteristics. The DBN-based machine learning method was used, and a model was trained to predict the sea state characteristics to compute the wave drift force. Zheng Wu[31] focused on 3-DOF wave energy convertor and established the relationship between the load resistance and power conversion efficiency based on machine learning. Shuo[32] used an Observed-Based Unknown Input Estimator(OBUIE) to es-

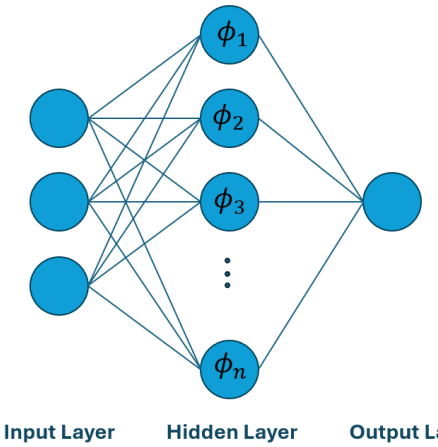

Figure 2.3: Radial Basis Functions Schematic Diagram

Table 2.2: Summary of three previous literature related to load estimation

Literature	Year	Method	Main Work	Limitation
Krishna Kumar et al.[25]	2018	DBN based ML model	Using Deep Belief Network (DBN) based ML method to predict the wave characteristic and derive the wave-induced loads	Only apply for long-term prediction
Zheng Wu et al.[31]	2022	EEMD and LSTM based ML model	Propose a load optimization control based on machine learning	Only focus on single device
Shuo Shi et al.[32]	2019	OBUIE and GP	Estimate the excitation force in time domain and predict the future forces using Gaussian Process	Does not perform well at sea state with low significant wave height

timate the excitation force, then a Gaussian Process is adopted to predict future value of the excitation force. The summary of these literatures are presented in Table 2.2

2.5. Review on the optimization of WEC Array Design

Several studies have been proposed on the optimization of WEC array design. Most of these studies look into a limited number of layouts, and then analyze each case by numerical modeling method to identify the optimal design. Borgarino[25] looked into the power absorption of a WEC farm with different layouts and interval distances between two absorbers. By comparing power production of square-based and triangle-based array, an optimal solution can be achieved. Moreover, Göteman[33] studied the impact of the dimension of PAs on the annual absorbed energy. The highlight of this research is the exploration of layouts involving PAs with different sizes. Apart from layout and distances between WECs, Bozzi[34] also studied the influence of different

Table 2.3: Summary of seven previous literature related to WEC array optimisation

Literature	Year	Method	Main Work	Limitation
B.Borgarino et al.[25]	2012	Numerical comparison	Investigate the power absorption of WEC farms with varying array shapes.	Insufficient number of shape tests
Malin Göteman et al.[33]	2017	Analytical and Numerical	Investigate how varying dimensions of WECs affect the annual power output of wave energy farms.	Does not account for the varying sea state during a year
Silvia Bozzi et al.[34]	2017	Numerical comparison	Investigate WEC farm power absorption with diverse array configurations, considering different wave directions	Lack of connection between total cost and power output
Alejandro et al.[39]	2018	Numerical comparison	Aiming to maximize the power output in a wave energy farm composed of 9 PAs in different array	Lack of connection between array and other design factor
E. Faraggiana et al.[40]	2019	Particle swarm(PSO) and GA	Aiming to minimize LCOE of WEC with different array	Cost estimation only based on part of the design
Mehdi Neshat et al.[38]	2020	Cooperative EA	Use multiple optimization methods to maximize the absorbed power	Long calculation time
Marianna et al.[36]	2020	Genetic Algorithm	Explore optimal array design considering cost and power production	Numbers of WECs is limited due to long calculation time

wave directions. The study not only showed the importance of aligning WECs with the dominant wave direction but also revealed that wave interaction could be negligible when the distance between two PAs is large.

In addition to simply comparing different results to achieve an optimal solution, other optimization methods are available. Genetic Algorithm is a commonly used method in WECs array design optimization. Jabrali [35] focused on the optimization of WEC parameters, such as the dimensions and PTO damping coefficient, using GA. Marianna[36] developed an economic model for a point absorber wave farm and used GA to identify the optimal array layout based on LCOE values. Chris [37] also explored the optimization of the array considering cost and power using GA. Additionally, Neshat[38] used multiple Evolution Algorithm (EA) strategies to validate the newly proposed Hybrid Cooperative Co-evolution Algorithm (HCCA) for array optimization. The highlights and the limitations of the above research are summarised in Table 2.3

3

Theory Background

The body motion of a WEC device in regular incoming waves is described by an equation of motion that accounts for both reaction and excitation forces. To solve this problem, potential flow theory is applied. Software like Capytaine uses the Boundary Element Method (BEM) to solve the Green function numerically, which enables the derivation of the potential on the surfaces of the floating bodies. Once the motion of the rigid body in a fluid is known, the mean power absorption of a single body point absorber can be determined.

The fundamental theorem of the numerical method will be presented in this chapter.

3.1. Basic Law of Fluid Mechanics

To describe the dynamic motion of a floating body, a fundamental understanding of fluid flow properties is necessary. The Navier-Stokes equations, which govern fluid motion, are crucial in this context. These equations consist of partial differential equations expressing the concepts of mass conservation, momentum conservation, and energy conservation.

3.1.1. Continuity Equation

The continuity equation is the application of mass conservation laws. It can be derived using the Reynold Transport Theorem (RTT) and Gauss Theorem. RTT provides a link between the conservation laws for a control volume and the conservation laws for a system of particles moving with the flow. The general RTT can be expressed as:

$$\frac{dB_{\text{system}}}{dt} = \frac{d}{dt}\int_{CV} \rho b \, dV + \int_{CS} \rho b \, \vec{V} \cdot \hat{n} \, dA \tag{3.1}$$

Where:

- B_{system} is the generic extensive property of the system (such as mass or momentum

- b is the corresponding intensive property (extensive property per unit mass)
- ρ is the fluid density.
- CV is the control volume
- CS is the control surface, the boundary of CV
- $\vec{V}$ is the velocity vector of the fluid.
- $\hat{n}$ is the unit normal vector pointing outward on the control surface

Gauss's Theorem is a key concept in vector calculus. It establishes a connection between the flux of a vector field through a closed surface and the divergence of the vector field within the volume enclosed by that surface. The theorem is given by:

$$\int_{CS} F \cdot n \, dS = \int_{CV} \nabla \cdot F \, dV \tag{3.2}$$

where:

- CS is the closed surface enclosing the volume CV.
- n is the outward-pointing unit normal vector on the surface.
- dS is a differential element of the surface.
- dV is a differential element of the volume.
- $\nabla \cdot \mathbf{F}$ is the divergence of the vector field F.

Substitute mass m into B_{system} in Equation 3.1, and transform the control surface term into control volume using Gauss Theorem yields the continuity equation:

$$\frac{\partial \rho}{\partial t} + \nabla \cdot (\rho \vec{V}) = 0 \tag{3.3}$$

For incompressible flow, the density ρ is a constant and therefore Equation 3.3 can be simplified as:

$$\nabla \cdot \vec{V} = 0 \tag{3.4}$$

3.1.2. Momentum Equation

The momentum equation is derived from Newton's second law and momentum conservation. With the application of RTT and Gauss Theorem again, the equation can be derived. Substitute momentum $m\vec{V}$ into B_{system} in Equation 3.1 yields the following formulation:

$$\sum \vec{F} = \int_{CV} \frac{\partial}{\partial t} \vec{V} \rho dV + \int_{CS} \vec{V} \rho \vec{V} \cdot \hat{n} dA \tag{3.5}$$

The $\sum \vec{F}$ term is a combination of forces acting on the fluid, including viscous stress, pressure, and external gravity force. Combine the term in the right hand using Gauss Theorem and decomposes the term in the left-hand side yields the momentum equation:

$$\rho\left(\frac{\partial V}{\partial t} + V \cdot \nabla V\right) = -\nabla p + \mu\nabla^2 V + \rho g \tag{3.6}$$

For non-viscous fluids, the $mu\nabla^2 V$ in the right-hand side in Equation 3.6 can be neglected, and yields the Euler Equation:

$$\rho(\frac{\partial \vec{V}}{\partial t} + \vec{V} \cdot \nabla \vec{V}) = -\nabla p + \rho g \tag{3.7}$$

3.1.3. Pressure and Force

The Bernoulli equation is an important concept that provides a relationship between the pressure, velocity, and elevation in a moving fluid. It is a simplification and rewrite of the Euler Equation along a streamline:

$$p = -\rho\frac{\partial \Phi}{\partial t} - \frac{1}{2}\rho(u^2 + v^2 + w^2) - \rho g z \tag{3.8}$$

Where Φ is the velocity potential. When considering the linear behavior of a floating body, the second term with higher order in Equation 3.8 can be neglected, which yields the linear pressure:

$$p = -\rho\frac{\partial \Phi}{\partial t} - \rho g z \tag{3.9}$$

In frequency domain, the pressure can be written as:

$$p = -i\omega\rho\phi - \rho g z \tag{3.10}$$

Once the fluid pressures surrounding the floating body are available, the forces that the floating body experiences can be obtained:

$$F = \iint_S (p \cdot \hat{n}) dS \tag{3.11}$$

Where S is the mean wetted surface of the floating body, $\hat{n}$ is the unit normal vector pointing outward of that surface. Considering 6-DOF body motion, the force in ith degree of freedom can be expressed as:

$$F_i = \iint_S (p \cdot n_i) dS \tag{3.12}$$

3.2. Potential Flow Theory

The theory background of Capytaine is based on the potential flow theory which is used to analyze the behavior of fluid flow under certain conditions. It is particularly useful for studying incompressible, irrotational, and non-viscous flows. The gradient of a given velocity field is the velocity potential. The velocity potential Φ is widely used for hydrodynamic analysis.

3.2.1. Velocity Potential

A velocity potential $\Phi(x, y, z, t)$ is a function where its derivative in any direction corresponds to the flow velocity in that direction. Assuming that the fluid is irrotational, non-viscous, incompressible, continuous, and homogeneous, the potential Φ is defined by:

$$\vec{V} = \nabla\Phi \tag{3.13}$$

$$u = \frac{\partial\Phi}{\partial x}, \quad v = \frac{\partial\Phi}{\partial y}, \quad w = \frac{\partial\Phi}{\partial z} \tag{3.14}$$

Where u, v, and w represent the velocity component in x, y, and z directions. Each velocity must still satisfy the continuity equation. Therefore Equation 3.4 is introduced and can be expressed as:

$$\frac{\partial u}{\partial x} + \frac{\partial v}{\partial y} + \frac{\partial w}{\partial z} = 0 \tag{3.15}$$

Apply the continuity equation and combine with Equation 3.14 yields the Laplace equation:

$$\nabla^2\Phi = \frac{\partial^2\Phi}{\partial x^2} + \frac{\partial^2\Phi}{\partial y^2} + \frac{\partial^2\Phi}{\partial z^2} = 0 \tag{3.16}$$

The potential flow can be easily superposition by adding simple potential elements to produce a more complicated flow. The most widely used potential flow element in ship hydrodynamics is the source flow. A source is a point from which flow radiates outward in all directions. The potential of a 3D source flow with source strength σ in spherical coordinate is given by:

$$\Phi = \int_S \frac{\sigma}{4\pi r} dS \tag{3.17}$$

3.2.2. Airy Wave Theory

Airy wave theory is a fundamental theory in fluid mechanics used to describe the propagation of waves on the water surface. The wave profile of the regular wave can be described by a simple harmonic function:

$$\eta(x, t) = \zeta cos(kx - \omega t) \tag{3.18}$$

Where:

- η is the wave elevation.
- ζ is the wave amplitude.
- k is the wave number ($k = \frac{2\pi}{\lambda}$)
- ω is wave frequency, measured in radians per second [rad/s].

Assuming the wave steepness is small and nonlinearity can be neglected, the wave potential can be obtained by solving the Laplace equation with the appropriate boundary conditions:

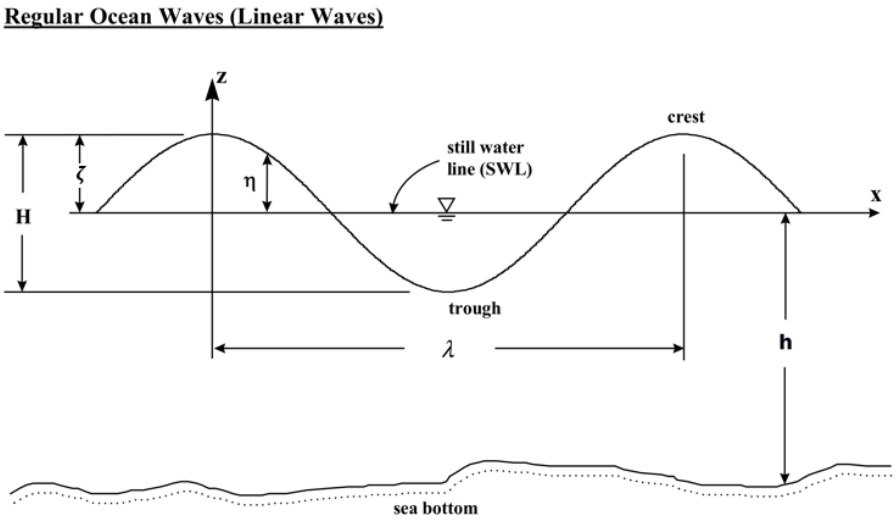

Figure 3.1: Regular wave diagram[41]

1. Free surface boundary condition: The pressure at the free surface is equal to the atmospheric pressure, and the moving speed of the surface and the fluid are identical

$$\begin{aligned} \frac{\partial \Phi}{\partial t} + g\eta = 0 \quad \text{at} \quad z = 0 \\ \frac{\partial \Phi}{\partial z} = \frac{\partial \eta}{\partial t} \quad \text{at} \quad z = 0 \end{aligned} \tag{3.19}$$

   Combine the above two equation yield the free surface boundary condition:

$$\frac{\partial^2 \Phi}{\partial t^2} + g\frac{\partial \Phi}{\partial z} = 0 \tag{3.20}$$

2. Seabed boundary condition: The seabed is impermeable, therefore the vertical velocity at the seabed must be zero

$$\frac{\partial \Phi}{\partial z} = 0 \quad \text{at} \quad z = -h \tag{3.21}$$

These conditions constitute the essential boundary conditions required to solve the Laplace equation. For a wave traveling in x direction, the solution of incoming Airy wave potential in the frequency domain can be expressed as:

- Shallow water

$$\phi_0 = -i\frac{g\zeta}{\omega}\frac{cosh(k(z+h)}{cosh(kh)}e^{ik(xcos\beta + ysin\beta)} \tag{3.22}$$

- Deep water

$$\phi_0 = -i\frac{g\zeta}{\omega}e^{kz}e^{ik(xcos\beta + ysin\beta)} \tag{3.23}$$

Where β is the incoming wave angle range from -2π to 2π, ζ is the wave amplitude, h is the water depth, and wave number k is given by dispersion relation $\omega^2 = kgtanh(kh)$. In deep water condition, the water depth h is infinity and the wave number k is defined by $\omega^2 = kg$

3.2.3. Potential Coefficient

Imagine a rigid body floating in a fluid with regular waves. The total potential of the floating body is the combination of the undisturbed incoming wave potential, the scattered wave potential, and the radiation potential:

$$\Phi = \Phi_r + \Phi_0 + \Phi_7 \tag{3.24}$$

Where:

- Φ_r represents the radiated wave potential caused by waves generated by body motion
- Φ_0 represents the incoming Airy wave potential
- Φ_7 is the scattered wave potential due to the presence of the fixed body

The potentials have to satisfy the following conditions:

1. Laplace equation
$$\nabla^2\Phi = \frac{\partial^2\Phi}{\partial x^2} + \frac{\partial^2\Phi}{\partial y^2} + \frac{\partial^2\Phi}{\partial z^2} = 0 \tag{3.25}$$
2. Free surface boundary condition
$$g\frac{\partial\Phi}{\partial z} - \omega^2\Phi = 0 \tag{3.26}$$
3. Seabed boundary condition
$$\frac{\partial\Phi}{\partial z} = 0 \quad \text{with} \quad z = -h \tag{3.27}$$

For frequency domain expression, the linear potential Φ can be expressed as the product of a space-dependent term and a harmonic time-dependent term with unit amplitude:

$$\Phi(x, u, z, t) = \mathfrak{Re}\left[\phi(x, y, z)e^{i\omega t}\right] \tag{3.28}$$

The complex amplitude of velocity potential ϕ is the superposition of the Airy wave potential ϕ_0, the scattered wave potential ϕ_7 and the radiation potential ϕ_j in six degree of freedom:

$$\phi = \phi_0 + \phi_7 + i\omega\sum_{j=1}^{6}\phi_j\hat{\zeta}_j \tag{3.29}$$

Where $\hat{\zeta}_j$ represents the complex amplitude of the harmonic body motion in jth degree of freedom. The added mass and radiation damping coefficients are defined as follows:

$$a_{ij} = \mathfrak{Re}\Big[\rho\iint_S \phi_j n_i dS\Big] \tag{3.30}$$

$$b_{ij} = \mathfrak{Im}\Big[-\rho\omega\iint_S \phi_j n_i dS\Big] \tag{3.31}$$

Where n_i is the unit normal direction of a surface element dS due to the motion in i degree of freedom. They are defined as follows:

$$\begin{aligned} surge: &\quad n_1 = cos(n,x) \\ sway: &\quad n_2 = cos(n,y) \\ heave: &\quad n_3 = cos(n,z) \\ roll: &\quad n_4 = yn_3 - zn_2 \\ pitch: &\quad n_5 = zn_1 - xn_3 \\ yaw: &\quad n_6 = xn_2 - yn_1 \end{aligned} \tag{3.32}$$

Where $cos(n,x)$ represents the cosine of the angle between the normal vector n and the x-axis, which is the same expression as: $\frac{n_x}{|n|}$

3.2.4. Solving Potentials

Radiation Problem

For different problem cases, the normal velocity on the body surface would vary. In the case of the radiation problem, the boundary condition at the hull surface is watertight, meaning that the normal velocity of the fluid around the hull matches the normal velocity of the hull itself for each degree of freedom. The normal velocity at a specific point on the hull surface is given by:

$$v_j = \dot{\zeta}_j \cdot \hat{n_j} \tag{3.33}$$

Where $\dot{\zeta}_j$ is the velocity in j degree of freedom, and $\hat{n_j}$ is the unit normal vector. Therefore, the hull boundary condition yields:

$$\frac{\partial \Phi_j}{\partial n} = v_j \tag{3.34}$$

Substitute Equation 3.28 in the left-hand side and transform the right-hand side yields:

$$\mathfrak{Re}\Big[\frac{\partial \phi_j}{\partial n} \cdot \hat{\zeta} \cdot e^{i\omega t}\Big] = \mathfrak{Re}\Big[\hat{\zeta} \cdot e^{i\omega t} \cdot n_i\Big] \tag{3.35}$$

$$\frac{\partial \phi_j}{\partial n} = n_j \tag{3.36}$$

Diffraction Problem

For the diffraction problem, the velocity on the floating body corresponds to the velocity of Airy's wave field. Since the hull surface is watertight, the sum of the incoming wave potential and the diffraction potential must equal zero.

$$\frac{\partial \phi_0}{\partial n} + \frac{\partial \phi_7}{\partial n} = 0 \tag{3.37}$$

Boundary Integral Problem

It is stated that the potential ϕ_j at a specific point on the mean wetted surface S, resulting from motion in the j degree of freedom and the diffraction potential ϕ_7, can be represented by a distribution of single sources across the body surface:

$$\phi_j(x) = \frac{1}{4\pi} \iint_S \sigma_j(\xi) \cdot G(x,\xi) dS \tag{3.38}$$

Where:

- $\phi_j(x)$ represents the potential function at a point x on the surface S
- $\sigma_j(\xi)$ represents the complex source strength at a source point ξ on the surface S
- $G(x,\xi)$ is the Green function which enables the potential due to a distribution of sources over the surface S satisfies the Laplace equation, the free surface condition, and the sea bottom condition.

Once the source strength $\sigma_j(\xi)$ is known the potential can be derived. The unknown source strengths $\sigma_j(\xi)$ for radiation and diffraction problems can be determined by applying corresponding boundary conditions on the body:

- For radiation boundary value problem

$$\frac{\partial \phi_j}{\partial n} = n_j = -\frac{1}{2}\sigma_j(x) + \frac{1}{4\pi}\iint_S \sigma_j(\xi)\cdot\frac{\partial G(x,\xi)}{\partial n}\cdot dS \tag{3.39}$$

- For diffraction boundary value problem

$$\frac{\partial \phi_7}{\partial n} = -\frac{\partial \phi_0}{\partial n} = -\frac{1}{2}\sigma_7(x) + \frac{1}{4\pi}\iint_S \sigma_7(\xi)\cdot\frac{\partial G(x,\xi)}{\partial n}\cdot dS \tag{3.40}$$

After solving the above equations the unknown source strengths and potential can be determined. Substituting the result into Equation 3.12, Equation 3.30, Equation 3.31 yields the hydrodynamic forces, added mass, and radiation damping respectively.

Numerical Method

In general, the hull shape of the floating body cannot be described by an analytical function, so the numerical aspect is introduced. By dividing the mean wetted surface of the body into N panels with uniformly distributed sources, the normal derivative of the potential at location m can be described as:

$$\frac{\partial \phi_{mj}}{\partial n} = -\frac{1}{2}\sigma_{mj} + \frac{1}{4\pi}\sum_{n=1}^{N}\sigma_{nj}\cdot\frac{\partial G_{mn}}{\partial n}\Delta S_n \quad \text{for} \quad m = 1,\ldots,N \quad \text{and} \quad n \neq m \tag{3.41}$$

This equation can be converted into a system of linear equations with N unknown complex source strengths.

For radiation problem

$$\begin{pmatrix} A_{11} & \cdots & \cdots & \cdots & A_{1N} \\ \cdots & A_{22} & \cdots & \cdots & \cdots \\ \cdots & \cdots & A_{33} & \cdots & \cdots \\ \cdots & \cdots & \cdots & \ddots & \cdots \\ A_{N1} & \cdots & \cdots & \cdots & A_{NN} \end{pmatrix} \begin{pmatrix} \sigma_{1,j} \\ \vdots \\ \vdots \\ \vdots \\ \sigma_{N,j} \end{pmatrix} = \begin{pmatrix} n_{1,j} \\ \vdots \\ \vdots \\ \vdots \\ n_{N,j} \end{pmatrix} \tag{3.42}$$

Where:

- j represents the degree of freedom of the radiation potential: $j = 1, ..., 6$

- $A_{nn} = -\frac{1}{2}$
- $A_{mn} = \frac{1}{4\pi}\frac{\partial G_{mn}}{\partial n}\Delta S_n$
- $\sigma_{n,j} =$ unknown source strength
- $n_{n,j} =$ is the local normal direction component at panel n in j degree of freedom given in Equation 3.32

For diffraction problem

$$\begin{pmatrix} A_{11} & \cdots & \cdots & \cdots & A_{1N} \\ \cdots & A_{22} & \cdots & \cdots & \cdots \\ \cdots & \cdots & A_{33} & \cdots & \cdots \\ \cdots & \cdots & \cdots & \ddots & \cdots \\ A_{N1} & \cdots & \cdots & \cdots & A_{NN} \end{pmatrix} \begin{pmatrix} \sigma_{1,7} \\ \vdots \\ \vdots \\ \vdots \\ \sigma_{N,7} \end{pmatrix} = \begin{pmatrix} -(\frac{\partial \phi_0}{\partial n})_1 \\ \vdots \\ \vdots \\ \vdots \\ -(\frac{\partial \phi_0}{\partial n})_N \end{pmatrix} \tag{3.43}$$

Where:

- $A_{nn} = -\frac{1}{2}$
- $A_{mn} = \frac{1}{4\pi}\frac{\partial G_{mn}}{\partial n}\Delta S_n$
- $\sigma_{N,7} =$ unknown source strength of diffraction potential at panel N

3.3. Rigid Body Motion

The motion of a rigid body is governed by the different external forces and by the inertia of the body itself. These forces can be derived by solving the boundary integral problems. After the forces are known, the rigid body motion can be predicted by setting up a proper equation of motion.

3.3.1. Total Forces

To estimate the motion of a body in fluid, it is essential to understand the forces acting on the hull surface. For a floating body in a moving fluid, the forces acting in the ith degree of freedom include the Froude-Krylov force, diffraction force, radiation force, and hydrostatic force. The first two forces are commonly referred to as excitation forces. In a linear analysis, it is assumed that the wave excitation force and the body's motion are decoupled, same as the radiation force and incoming waves. This means the forces experienced by the body due to its motion are independent of the waves, and the forces due to the waves are independent of the body's motion. Consequently, the total force can be described as the simple sum of these four components:

$$F = \sum_{i=1}^{6} \left(\underbrace{F_{FK,i} + F_{d,i}}_{\text{Excitation Force}} + F_{r,i} + F_{s,i} \right) \tag{3.44}$$

The Froude-Krylov force F_{FK} is generated from the unsteady pressure field generated by undisturbed incoming waves, while the radiation force F_r is due to the waves

produced by the body's motion. Furthermore, the diffraction force F_d is caused by wave disturbances resulting from the presence of the stationary body. Lastly, the hydrostatic force F_s, resulting from buoyancy, is the only term that is not related to the fluid's dynamic behavior around the hull of the floating body. Once the potentials are solved, the total pressure p can be derived by substituting Equation 3.29 into Equation 3.10:

$$p = -i\rho\omega \left(\phi_0 + \phi_7 + i\omega \sum_{i=1}^{6} \phi_i \hat{\zeta}_i \right) - \rho g z \tag{3.45}$$

With the application of Equation 3.12, the total force in ith degree of freedom can be written as:

$$F_i = \iint_S \left[-i\omega\rho \left(\phi_0 + \phi_7 + i\omega \sum_{i=1}^{6} \phi_i \hat{\zeta}_i \right) - \rho g z \right] n_i dS \quad \text{for} \quad i = 1, ..., 6 \tag{3.46}$$

This expression can be further decomposed into the summation of excitation force, radiation force, and hydrostatic force:

$$F_i = \underbrace{-i\omega\rho \iint_S (\phi_0 + \phi_7)\, n_i dS}_{\text{Excitation Force}} + \underbrace{\rho\omega^2 \iint_S \left(\sum_{i=1}^{6} \phi_i \hat{\zeta}_i \right) n_i dS}_{\text{Radiation Force}} - \underbrace{\rho g \iint_S z n_i dS}_{\text{Hydrostatic Force}} \tag{3.47}$$

3.3.2. Excitation Force

When a wave approaches a floating body, the pressure field is disturbed by the incoming wave potential, which leads to the generation of excitation forces. These forces are a combination of the Froude-Krylov force and the diffraction force. The Froude-Krylov force arises from the velocity potential of the undisturbed incident wave and is calculated by integrating the pressure distribution over the mean wetted surface of the body. This can also be seen as the incoming wave potential remains unchanged and ignores the presence of the body. Conversely, the diffraction force, which results from the diffracted wave potential across the wetted surface, acts as a corrected term to the Froude-Krylov force because of the body's presence. The contribution of the incoming wave potential and diffraction potential extracted from Equation 3.45 can be expressed as:

$$p_{EX} = -i\rho\omega(\phi_0 + \phi_7) \tag{3.48}$$

Substitute this formulation into Equation 3.12 yields the excitation force.

$$F_{EX,i} = -i\omega\rho \iint_S (\phi_0 + \phi_7)\, n_i dS \tag{3.49}$$

3.3.3. Radiation Force

A moving body in a fluid will generate waves that radiate outward. This wave would gradually dissipate after traveling over an infinite distance. This energy loss is captured by a damping force that opposes the body's motion. Additionally, as the body moves, it causes a small portion of the surrounding water to oscillate from crest to trough. Since this portion of water accelerates at the same rate as the moving body,

the resulting additional net force can be captured by the added mass. The pressure correspond to the radiation potential can be extracted from Equation 3.45:

$$p_R = \rho\omega^2 \left(\sum_{i=1}^{6} \phi_i \hat{\zeta}_i \right) \tag{3.50}$$

Substitue the pressure into Equation 3.12 yields the radiation force:

$$F_{R,i} = \rho\omega^2 \iint_S \left(\sum_{i=1}^{6} \phi_i \hat{\zeta}_i \right) n_i dS \tag{3.51}$$

This expression can also be rewritten as:

$$F_{R,i} = \sum_{j=1}^{6} \hat{\zeta}_i f_{ij} \qquad i = 1, ..., 6 \tag{3.52}$$

Where f_{ij} is the complex force in ith degree of freedom induced from the velocity of the structure in j direction. f_{ij} can be written as:

$$f_{ij} = \omega^2 a_{ij} - i\omega b_{ij} \tag{3.53}$$

Where a_{ij} and b_{ij} are the added mass and radiation damping coefficient defined in Equation 3.30 and Equation 3.31 respectively. In other words, the radiation forces are incorporated into the equation of motion through the added mass and radiation damping coefficient matrices, as shown in Equation 3.59.

3.3.4. Hydrostatic Force

The hydrostatic force, also known as the buoyancy force, is the force acting on the floating body which is proportional to the submerged volume of the body.The pressure corresponding to hydrostatic force can be extracted from Equation 3.45:

$$p_S = -\rho g z \tag{3.54}$$

Substitute the pressure into Equation 3.12 yields the hydrostatic force:

$$F_{S,i} = -\rho g \iint_S z \cdot n_i dS \tag{3.55}$$

When calculating the hydrostatic force using the above equation, the force is considered zero-order, meaning that it is independent of the floating body's motion. However, in reality, this force is balanced by the weight of the structure and is influenced by the body's movement. This motion-dependent hydrostatic force is referred to as the restoring force and can be expressed as:

$$F_{S,i} = -\sum_{j=1}^{6} c_{ij} \zeta_i \quad i = 1, ..., 6 \tag{3.56}$$

Where ζ_i is the motion of the body in ith degree of freedom, and c_{ij} represents the restoring coefficient. For a rigid body the restoring coefficient can be calculated by:

$$\begin{aligned}
c_{33} &= \rho g \iint_S n_3 dS \\
c_{34} &= \rho g \iint_S y n_3 dS \\
c_{35} &= -\rho g \iint_S y n_3 dS \\
c_{44} &= \rho g \iint_S y^2 n_3 dS - \rho g \forall z_b + m g z_g \\
c_{45} &= -\rho g \iint_S x y n_3 dS \\
c_{46} &= -\rho g \forall x_b + m g x_g \\
c_{55} &= \rho g \iint_s x^2 n_3 dS + \rho g \forall z_b - m g z_g \\
c_{66} &= -\rho g \forall y_b + m g y_g
\end{aligned} \tag{3.57}$$

These coefficients constitute the hydrostatic coefficient matrix K, and the hydrostatic force is incorporated into the equation of motion through this matrix.

The center of buoyance of the floating body in Cartesian coordinates can be calculated by:

$$\begin{aligned}
x_b &= \frac{1}{\forall} \iiint_{\forall} x dV \\
y_b &= \frac{1}{\forall} \iiint_{\forall} y dV \\
z_b &= \frac{1}{\forall} \iiint_{\forall} z dV
\end{aligned} \tag{3.58}$$

Where $\forall$ represents the submerged volume of the body.

3.3.5. Equation of Motion

Once the total forces are derived, the motion of the body can be predicted using a mass-spring-damper system. This system includes an inertia term that resists acceleration, a damping term that dissipates energy, and a spring term that represents the restoring force. The mass-spring-damper system includes the excitation force can be written as:

$$(M + A)\ddot{X} + B\dot{X} + KX = F \tag{3.59}$$

Here M is the 6x6 mass matrix representing the inertia of the floating body. Additionally, A is the added mass matrix of the same dimension, and B is the radiation damping matrix. the coefficients of added mass matrix and radiation damping are defined in Equation 3.30 and Equation 3.31 respectively. Lastly, K is the hydrostatic stiffness matrix whose coefficients are defined in Equation 3.57. The mass matrix M

can be expressed as:

$$M = \begin{pmatrix} m & 0 & 0 & 0 & mz_g & -my_g \\ 0 & m & 0 & -mz_g & 0 & mx_g \\ 0 & 0 & m & my_g & -mx_g & 0 \\ 0 & -mz_g & my_g & I_{11} & I_{12} & I_{13} \\ mz_g & 0 & -mx_g & I_{21} & I_{22} & I_{23} \\ -my_g & mx_g & 0 & I_{31} & I_{32} & I_{33} \end{pmatrix} \tag{3.60}$$

Where m is the mass of the body. x_g, y_g, and z_g are the coordinate of the center of gravity. The motion of the body can be expressed in the frequency domain as:

$$X = \hat{\zeta} e^{i\omega t} \tag{3.61}$$

Where $\hat{\zeta}$ represents the complex amplitude of the body motion. With this expression, the body acceleration and the velocity can also be written in frequency domain:

$$\dot{X} = i\omega \hat{\zeta} e^{i\omega t} \tag{3.62}$$

$$\ddot{X} = -\omega^2 \hat{\zeta} e^{i\omega t} \tag{3.63}$$

Consequently, the overall equation of motion in frequency domain becomes:

$$\left[-\omega^2(M + A) + i\omega B + K\right] \hat{\zeta} e^{i\omega t} = F \tag{3.64}$$

To find the natural frequency, the right-hand side of the above equation is set to zero. Then, the natural frequency can be derived by finding the ω which fulfills the following equation:

$$\left[-\omega^2(M + A) + i\omega B + K\right] \hat{\zeta} e^{i\omega t} = 0 \tag{3.65}$$

For the nontrivail case($\hat{\zeta} \neq 0$), the natural frequency ω_n fulfill the following equation:

$$-{\omega_n}^2 + \frac{K}{M + A(\omega_n)} = 0 \tag{3.66}$$

Once the mass matrix, added mass matrix, radiation damping matrix, hydrostatic matrix, and excitation force are determined, the motion of the body can be predicted. By combining these values, the response amplitude operator (RAO) can be calculated, which is defined as:

$$RAO = \frac{\hat{\zeta}}{\hat{\zeta_a}} \tag{3.67}$$

Where $\hat{\zeta_a}$ is the complex amplitude of the incoming wave. The RAO can be used to compute the response motion of the floating body in 6 degree of freedom. For regular wave, the response motion is the wave amplitude times the RAO at each degree of freedom.

Since The excitation force is proportional to the incoming wave amplitude $\zeta_a = \hat{\zeta_a} e^{i\omega t}$, Equation 3.64 can also be expressed as:

$$\left[-\omega^2(M + A) + i\omega B + K\right] \hat{\zeta} e^{i\omega t} = F \cdot \hat{\zeta_a} e^{i\omega t} \tag{3.68}$$

Consequently, the RAO can be obtained using the following equation:

$$RAO(\omega) = [-\omega^2(M + A) + i\omega B + K]^{-1} F(\omega) \tag{3.69}$$

3.4. Power Absorption

Power production is a critical parameter for evaluating the performance of a WEC. For a single-body point absorber, the heave motion is the most significant among all six degrees of freedom, since only the heave motion drives PTO system and generates power. Furthermore, research indicates that selecting the optimal PTO damping coefficient can maximize the production of wave energy.

3.4.1. Mean Power Absorption

As waves propagate through the WECs, the motion of the buoy drives the damper of the PTO system and generates power. During a wave cycle, the mean power absorption is equivalent to the average power utilized by the mechanical damper within the PTO system. Consequently, if the wave is assumed to be harmonic, the mean absorbed power over a wave cycle can be expressed as:

$$P = \frac{1}{T}\int_0^T B_{PTO}u^2 dt = \frac{1}{2}\omega^2 B_{pto}|\zeta_3|^2 \tag{3.70}$$

Where B_{PTO} represents the damping coefficient of the PTO device, and ζ_3 represents the heave amplitude of the WEC.

3.4.2. Suboptimal Power control

The suboptimal PTO control is a principle that maximizes the power absorption expressed in Equation 3.70. This approach incorporates the concept of impedance [42][43], which is an analogy to its use in electric systems. The radiation impedance, denoted by Z, is defined as:

$$Z = -i\omega\rho \iint_S \phi_3 \cdot n_3 dS \tag{3.71}$$

Where ϕ_3 is the radiation potential component in heave degree of freedom. Consequently, the radiation force of the heave mode can be written as:

$$F_r = i\omega Z\hat{\zeta_3} = R + iX \tag{3.72}$$

Where $\hat{\zeta_3}$ represents the complex heave amplitude. The optimum PTO damping coefficient can be derived using the following equation:

$$\begin{aligned} B(\omega)_{PTO} &= |Z_i| \\ &= \left[R_i(\omega)^2 + X_i(\omega)^2\right]^{\frac{1}{2}} \end{aligned} \tag{3.73}$$

Where:

$$R_i(\omega) = B_a(\omega) + R_f \tag{3.74}$$

$$X_i(\omega) = i\omega\left[m + a_{33}(\omega)\right] + \frac{c_{33}}{i\omega} \tag{3.75}$$

- Z_i is the intrinsic impedance of the heaving body
- R_i is the real part of the intrinsic impedance

- X_i is the imaginary part of the intrinsic impedance
- B_a is the radiation damping at certain wave frequency
- R_f is the term accounting for the viscous loss
- m is the mass of the floating body
- a_{33} is the heave added mass at certain wave frequency
- c_{33} is the restoring coefficient

The nonlinear viscous term R_f, derived from Morrison's equation, can be linearized using a Fourier series expansion based on work from Malta et al.[44]. Combining all the parameters in the above equation yields the optimal power-damping coefficient at a certain wave frequency.

4

Methodology

In this chapter, the methodology and the process to find the optimal array design is presented. The response motion of a WEC in regular waves is estimated using potential flow theory and Newton's second law. The hydrodynamic analysis is performed with Capytaine, and once the body's motion is determined, the power output of the WEC is computed using Matlab. This process is repeated with the added devices to evaluate an array of four WECs. By varying the design parameters and collecting data on power production, relationships between parameters can be analyzed. Once these relationships are established, the optimal array design can be determined.

4.1. Model Setup

In this thesis, a single-device point absorber with a cylindrical shape is selected as the test model. The geometry is created using the CAD software Rhinoceros 3D[45]. After creating the model in Rhino, it is exported as a .stl file, which can then be read into Capytaine for setting up a `FloatingBody`. The full geometry of the model is shown in Figure 4.1 and the mesh below water plane is shown in Figure 4.2

The test point absorber is cylindrical, with a diameter of 4 meters and a height of 10 meters. A `FloatingBody` contains information of mesh, degree of freedom, and physical properties such as mass and center of mass. Note that only the submerged part of the model is used for hydrodynamic analysis.

4.2. Radiation & Diffraction Analysis

Once a floating body is created the next step is to define `LinearPotentialFlowProblem`, which is a defined class in Capytaine and is also a problem collection of several parameters such as the wave angular frequency ω, water density ρ, and water depth h. The `LinearPotentialFlowProblem` class has two sub-classes: `RadiationProblem` and `DiffractionProblem`. These two types of problems require different necessary parameters and solve the Green function with corresponding boundary conditions. For the radiation problem, the necessary parameters include the mesh, degree of freedom,

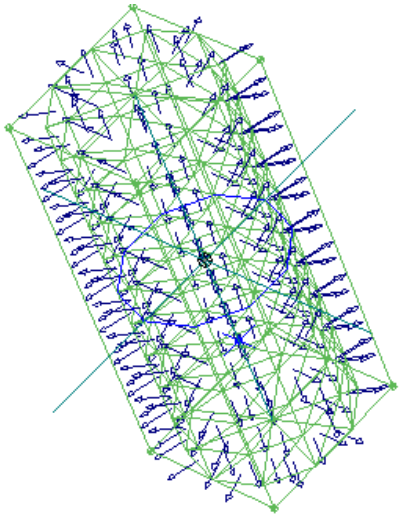

Figure 4.1: Full geometry of test point absorber shown in BEMRosetta

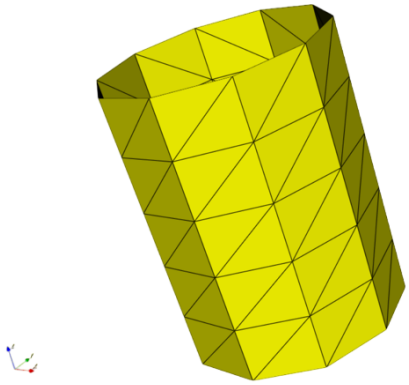

Figure 4.2: Submerged part of the mesh shown in Capytaine

and the incoming wave frequency. For the diffraction problem, the necessary parameters are mesh, wave angle, and wave frequency. By configuring these problems with various parameters and running them multiple times, several key hydrodynamic characteristics can be determined.

4.3. Data Analysis

4.3.1. Linear Regression

The goal of performing data analysis is to find the relationship of input parameter and the output power and forces. For property that involves single parameter like forces, the linear regression is used to setting up the relationship between forces and input parameters. The work is conducted in Matlab using the first-order polyfit function [46].

Table 4.1: Summarized characteristic of the buoy model

Feature	Value	Unit
Diameter	4	[m]
Height	10	[m]
Mass	62831	[kg]
Natural frequency	1.22091	[rad/s]
PTO damping coefficient	29	[kNs/m]
Number of panels	220	[-]
Number of nodes	112	[-]

4.3.2. Machine Learning Method

When a property involves two or more parameters, linear regression cannot clearly show the relationship between the parameters and the output data. To address this limitation, machine learning is employed. By training a model using machine learning, relationships involving multiple inputs can be more accurately determined.

In this thesis, the `scikit-learn` (sklearn) Python package was used for machine learning analysis. This package enables the application of both Random Forest Regressor and Neural Network. For the Random Forest Regressor, key parameters include `n_estimators`, which specifies the number of trees, and `random_state`, which controls the randomness of the sampling process used to build the trees. Setting `random_state` to a constant ensures that the model produces identical results each time it is run. The sklearn package also provides the Multi-Layer Perceptron (MLP) for neural network analysis. The `hidden_layer_sizes` parameter determines the number of neurons in each hidden layer, while the `max_iter` parameter controls the maximum number of iterations for the optimization algorithm to converge. If the model fails to converge within this limit, training will stop, and it means that further adjustments are required to improve convergence. After training the machine learning models, the optimal array design can be determined by repeatedly running the model and predicting the output multiple times.

5

Numerical Results Using Capytaine

Capytaine is an open-source Python package frequency-domain BEM solver, adapted from NEMOH. It can be used for the computation of wave loads on the floating structure. Besides the various function in Capytaine, the Python programming environment makes it easier to perform further analysis after obtaining hydrodynamic results. The process of solving a problem in Capytaine starts with setting up a model used in the analysis, followed by defining a linear potential flow problem with appropriate parameters. After solving the problem, the results are saved for further analysis.

5.1. Single device in Heave Mode

5.1.1. Hydrodynamic Result for Single Device

Once the floating body is set, the multiple problems with different input wave frequencies can be solved in a loop. The frequency range is divided into 100 uniform values between 0.01 and 10, and the wave direction is zero. After solving all the `LinearPotentialFlowProblem`, the result can be visualized by line plots shown in Figure 5.3

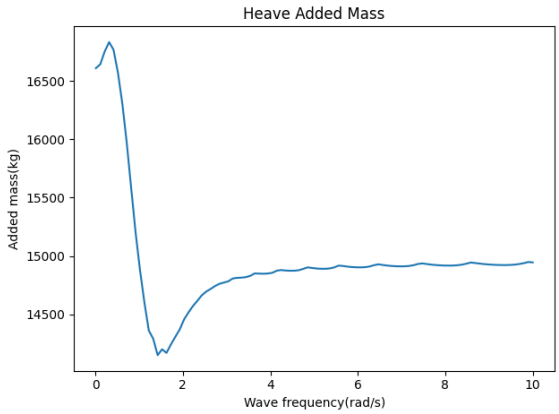

Figure 5.1: Heave added mass

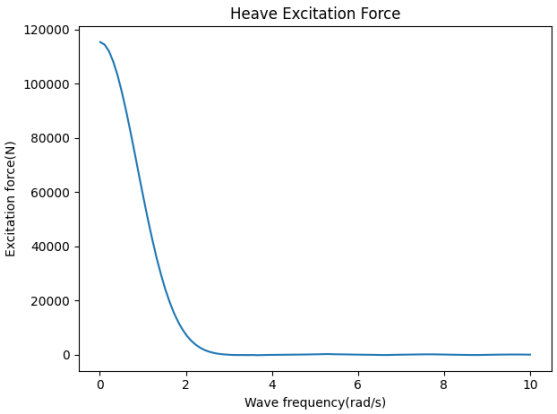

Figure 5.2: Heave excitation force

Figure 5.3: Hydrodynamic characteristic for single device

It can be seen from the figures that both added mass and excitation force has a larger variance at lower frequencies and coverge at higher frequencies.

5.1.2. RAO Computation

Capytaine offers a default module for computation of Response Amplitude Operator. the `rao` function receives the xarrayDataset containing the result of previous hydrodynamic problems and return the RAO result stored in the xarrayDataArray. The RAO in the heave direction calculated based on the default function is shown in Figure 5.4

5.1.3. Power Production

In the simulation analysis of the output power of a WEC, the natural frequency is an important factor to verify the power output and controlling factors during the design process of the device. The natural frequency is the value that makes Equation 3.66 equals zero. The figure used for derivation of the natural frequency is shown in Figure 5.5

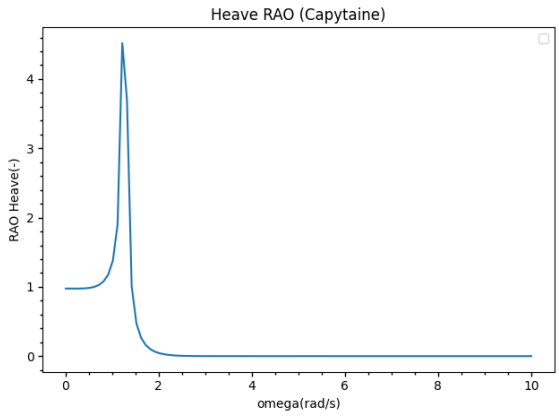

Figure 5.4: RAO in heave direction

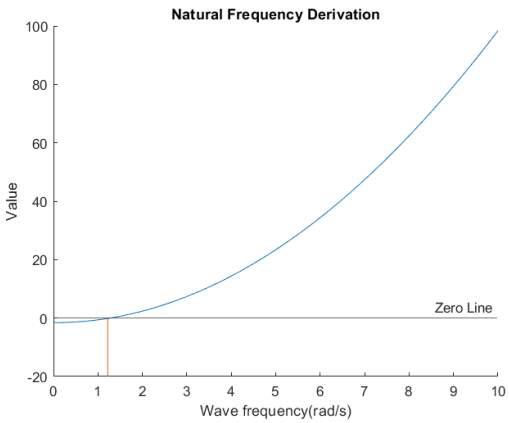

Figure 5.5: Natural frequency derivation

The figure clearly shows that the blue line intersects between wave frequencies 1

and 2. With closer inspection, the natural frequency is determined to be 1.22.

To estimate the power output of the WEC device in the regular wave, the linear PTO was included to the model. In this thesis, $29000[Ns/m]$ was selected as the PTO damping coefficient as it is the optimal damping coefficient under the natural frequency of the device[43] With the usage of Equation 3.70, the power matrix of the single device can be obtained in Figure 5.6

Figure 5.6: Power matrix of the single device

Based on the power matrix figure, the maximum power occurs at a period of 5 seconds, which coincides with the natural frequency.

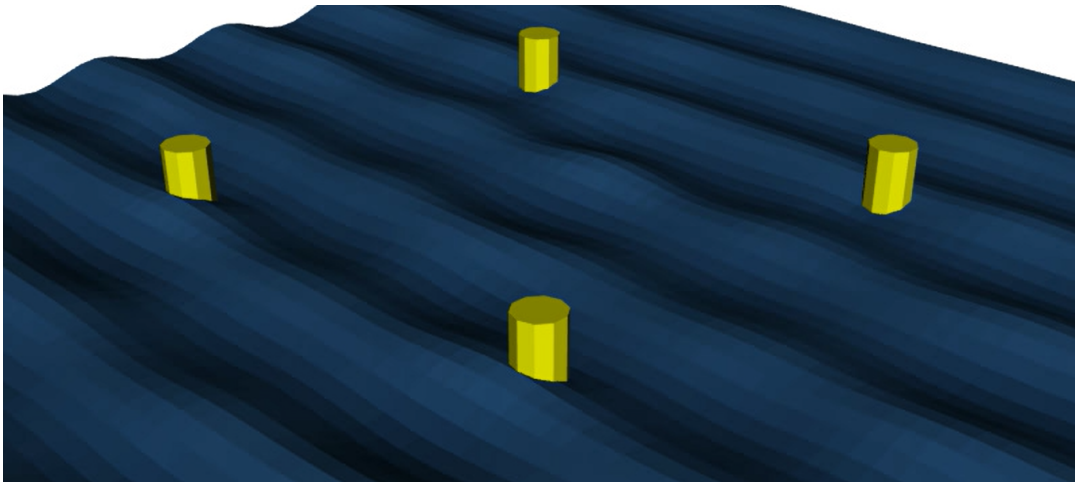

Figure 5.7: Multiple devices array configuration (array spacing = 40m)

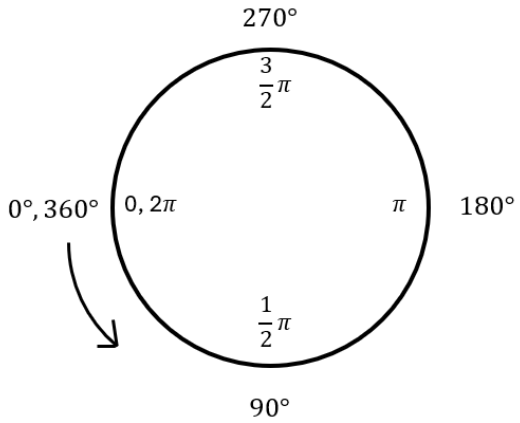

Figure 5.8: Wave direction

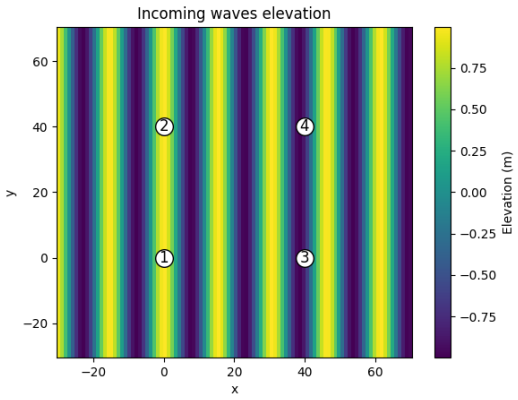

Figure 5.9: Array configuration and incoming wave configuration (wave direction angle=0°)

5.2. Multiple device

5.2.1. Derivation of Hydrodynamic Characteristics

For the purpose of finding the optimal array design, multiple bodies should be included in the Capytaine to determine the hydrodynamic characteristic. To reduce the memory load in the further machine learning analysis, only the heave degree of freedom is added each of the floating body. The array design is selected as a square shape for several reasons. The first reason is that a square shape has fewer factors when compared to complex shapes, which is crucial to perform machine learning. Additionally, a square array is less sensitive to wave direction, making the results applicable to a wider range of sites. The tested wave farm is composed of 4 identical single device point absorbers used in section 5.1. The configuration of the wave farm is shown in Figure 5.7. The parameters of the analysis include a frequency range divided into 100 uniform values between 0.01 and 10, a wave direction of zero, and a spacing of 40 meters (10 times the diameter) between each device. The RAO in heave direction and hydrodynamic characteristics for each device are shown in Figure 5.10 and Figure 5.13.

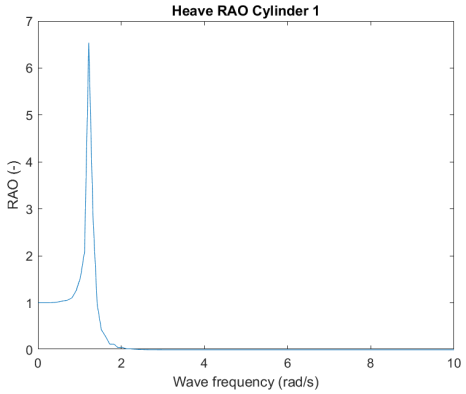

(a) Device 1

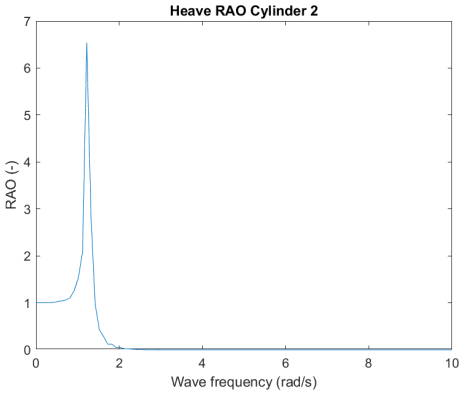

(b) Device 2

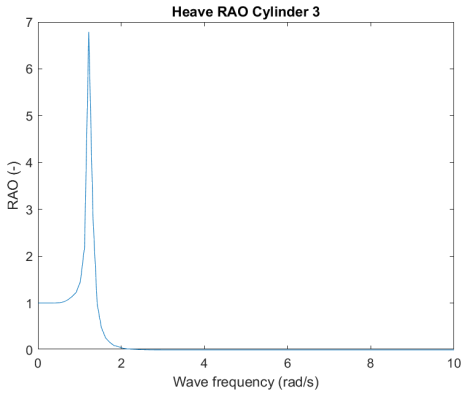

(c) Device 3

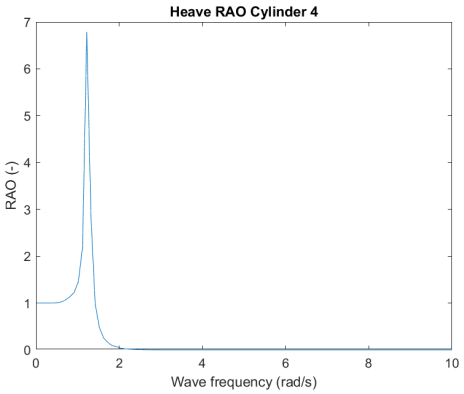

(d) Device 4

Figure 5.10: Heave RAO for each device of the array

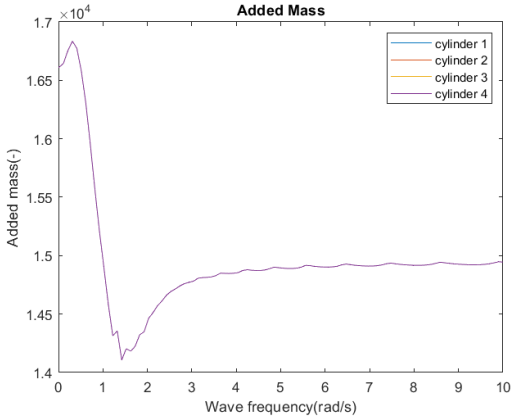

Figure 5.11: Heave added mass

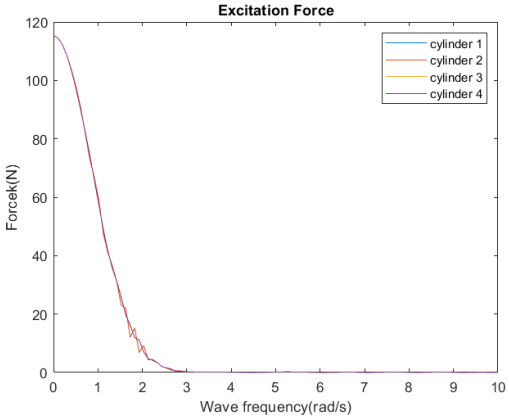

Figure 5.12: Heave excitation force

Figure 5.13: Hydrodynamic characteristic for each device in the wave farm

5.2.2. Derivation of Wave Field

To better understand the wave-structure interaction among the four devices, an analysis of the radiation field and the diffraction field is included. The radiation field repre-

sents the elevation caused by the radiated waves generated from the moving devices in each degree of freedom. Since each device is only allowed to move in heave direction, the radiation field of the array therefore has four degree of freedom. The results are shown in Figure 5.14 and Figure 5.15. To better illustrate the elevation, a wave frequency of 2 rad/s and 1 rad/s are selected.

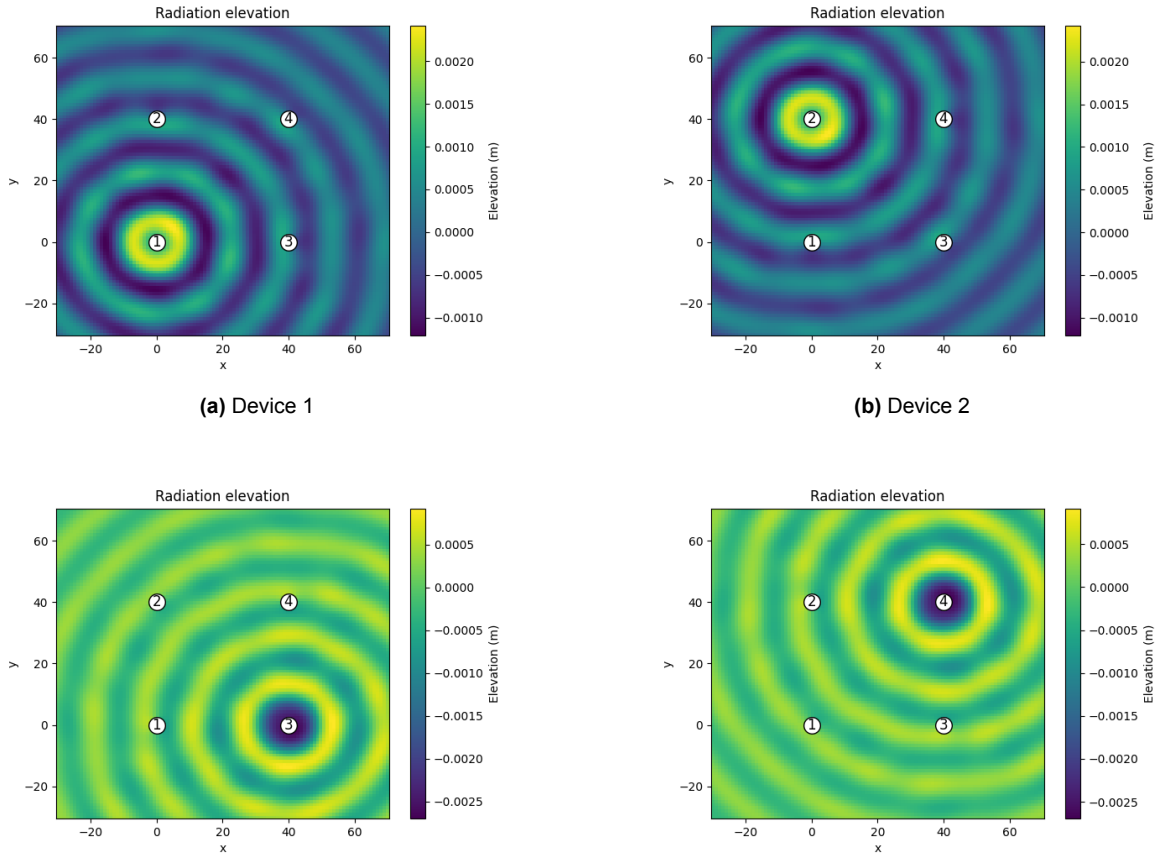

(a) Device 1

(b) Device 2

(c) Device 3

(d) Device 4

Figure 5.14: Radiation Field $\omega = 2$

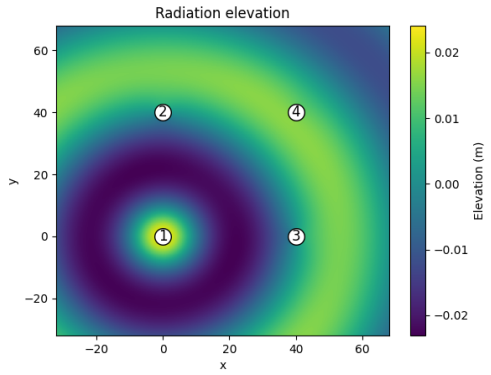

(a) Device 1

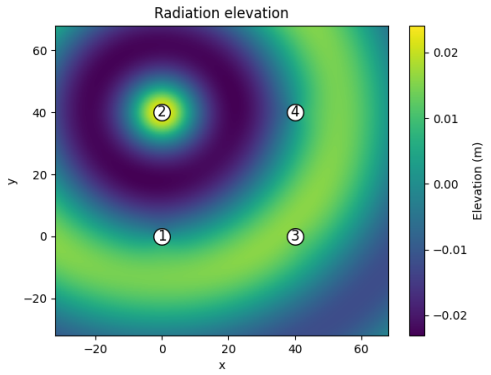

(b) Device 2

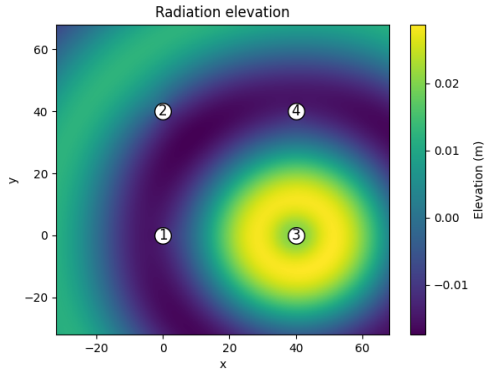

(c) Device 3

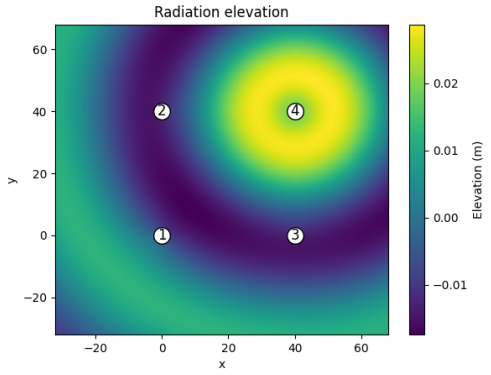

(d) Device 4

Figure 5.15: Radiation Field $\omega = 1$

The diffraction field represents the elevation caused by diffracted waves. In the simulation, the wave angle is set to zero radians. In Capytaine, a wave direction of zero radians propagates from the negative x to the positive x direction, which mean from left to the right. The result of the diffraction wave fields for wave frequency equal to 1 and 2 rad/s are shown in Figure 5.18

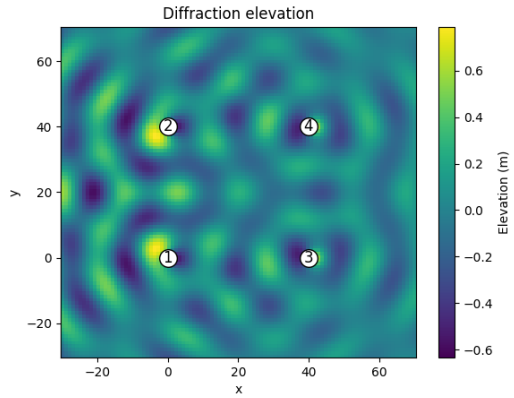

Figure 5.16: Diffraction field $\omega = 2$

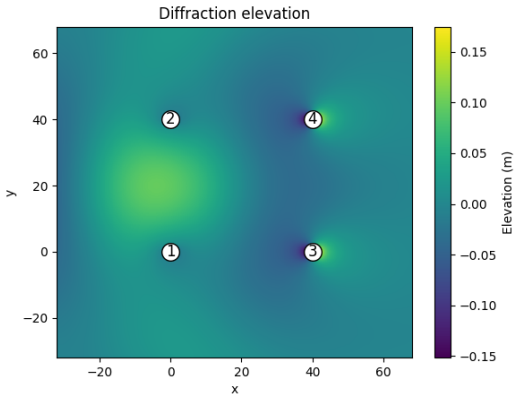

Figure 5.17: Diffraction field $\omega = 1$

Figure 5.18: Diffraction Field

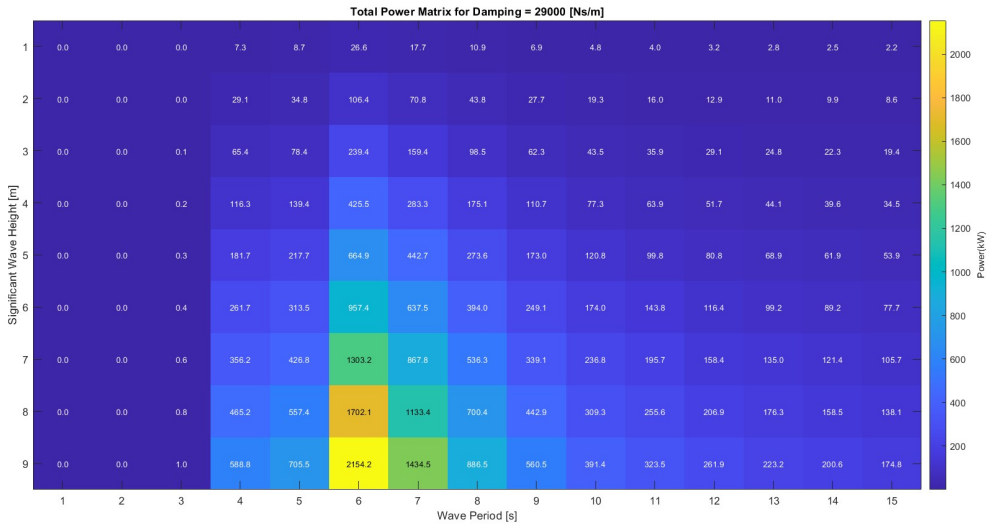

Figure 5.19: Power Matrix of The Wave Farm

The power production of the wave farm, consisting of four individual devices, can be computed by calculating the heave amplitude of each device and using Equation 3.70. The power matrix of the wave farm is shown in Figure 5.19. Compared Figure 5.19 with Figure 5.6, the period where the maximum power output occurs shifts from 5 seconds to 6 seconds. This shift indicates that there exist a significant difference between modelling of a single device and multiple devices. The interactions within the wave farm can alter the natural frequency of individual devices.

6

Finding the Relationship

In this chapter, the relationship between array configuration and power output, as well as excitation force, will be discussed using linear regression. The array spacing is selected as an input variable to analyze this relationship. The spacing ranges from 2 times the diameter of the device to 12 times the diameter, with increments of 2D. Additionally, the wave direction angle is included as another input, varying from 0 to 90 degrees in 45-degree increments

6.1. Determine the Relation of Load between design parameters Using Linear Regression

The regression analysis is performed in Matlab using `polyfit` function. Due to the limitation of linear regression, which restricts the input variable to only one, the results and the linear polynomial lines are displayed as three individual lines. Besides, the excitation force on different device is displayed in individual figures. The results for spacing equals 8 meters and 40 meters are shown in Figure 6.1 and Figure 6.2. The linear polynomial fit line shows a trend similar to the original data. The excitation force on devices 1 and 4 does not exhibit significant variance when the wave direction changes. However, the excitation force on devices 2 and 3 shows slight changes with varying wave direction angles.

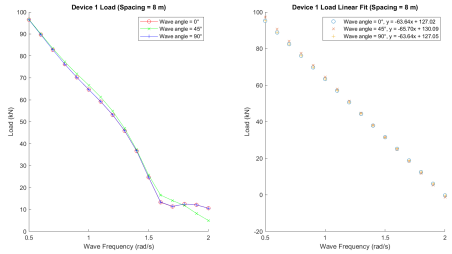

(a) Device 1

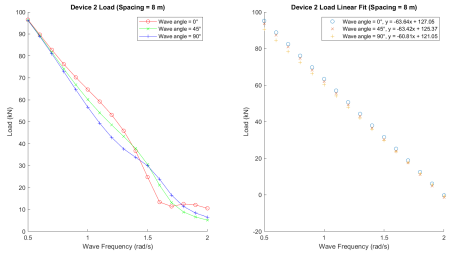

(b) Device 2

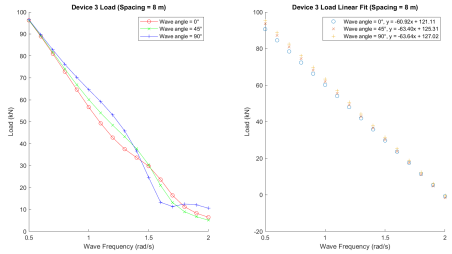

(c) Device 3

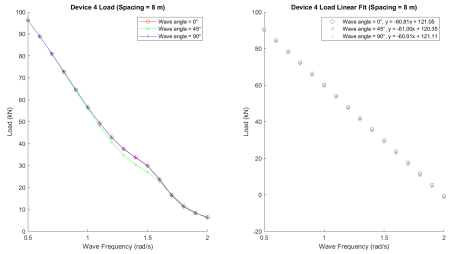

(d) Device 4

Figure 6.1: Excitation Force at spacing = 8 meters

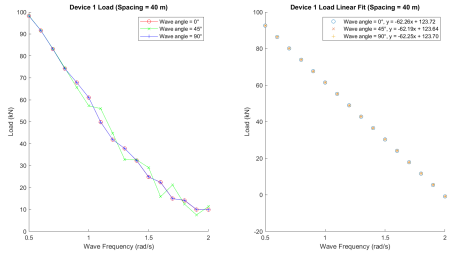

(a) Device 1

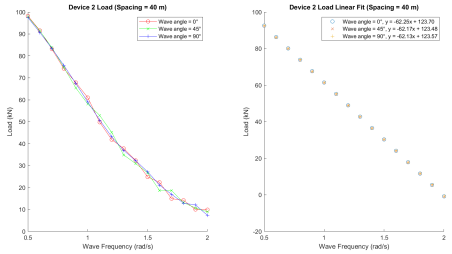

(b) Device 2

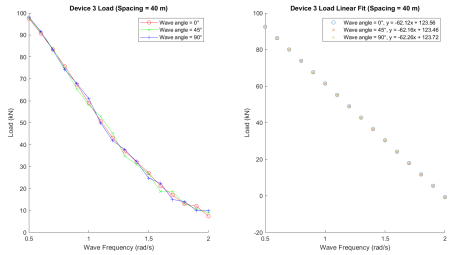

(c) Device 3

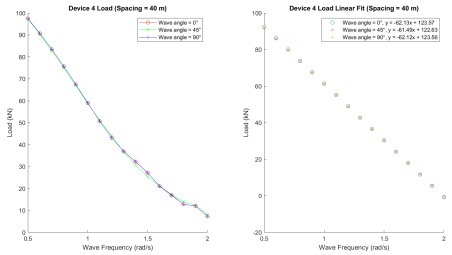

(d) Device 4

Figure 6.2: Excitation Force at spacing = 40 meters

The regression analysis of the overall power output is also performed in Matlab. For power production, a cubic polynomial fit curve wass used to describe the variance of the power. The results are shown in Figure 6.3 and Figure 6.4. The results implied that as the input variables increase the regression analysis is no longer reliable for determining the relation between power and array configuration.

By combining all the linear equations with different array spacing using linear regression analysis, the general mathematical formulation for specific angle and device

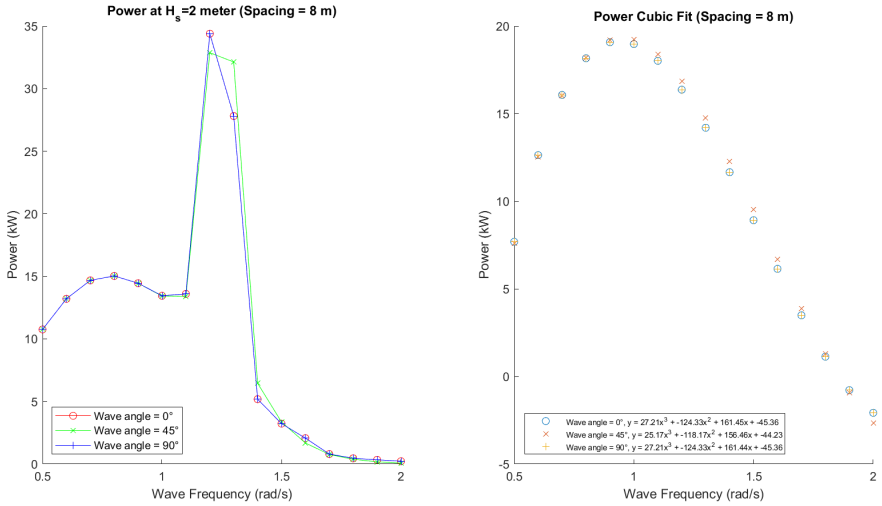

Figure 6.3: Power analysis for spacing = 8 meters

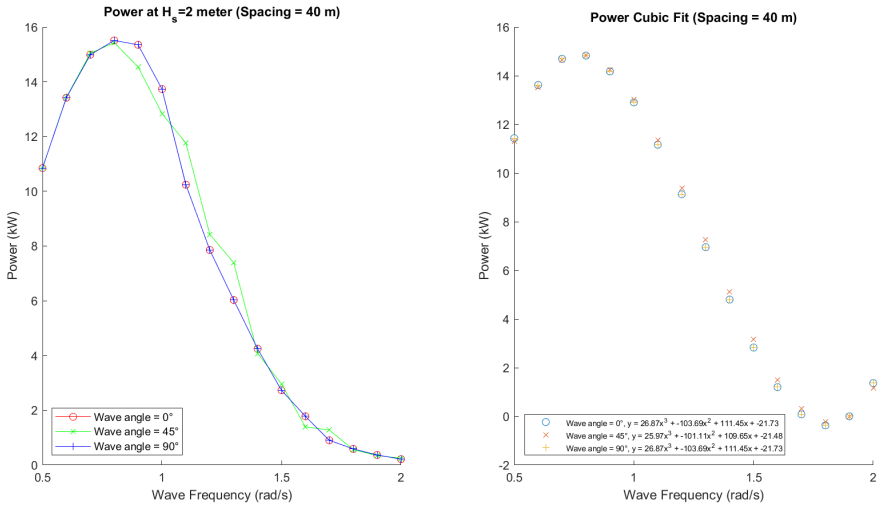

Figure 6.4: Power analysis for spacing = 40 meters

index can be derived. For device 1 at wave incoming direction angle equals to zero, the relation can be expressed as:

$$F_{ex}(x, y) = (0.041 \cdot x - 64.166) \cdot y + (-0.084 \cdot x + 127.31) \tag{6.1}$$

Where:

- x is the array spacing [m]
- y is the wave frequency [rad/s]
- F_{ex} is the heave excitation force on the device [kN]

To evaluate the reliability of this mathematical formulation, the value generated by Equation 6.1 is compared to the original data, and the summarized results are presented in Table 6.1:

Table 6.1: Evaluation of the estimated forces

Wave Frequency [rad/s]	Original Data [kN]	Predicted Data [kN]	Error [%]
0.5	98.25	92.68	5.66
0.6	91.58	86.43	5.62
0.7	83.16	80.18	3.59
0.8	74.24	73.92	0.43
0.9	67.88	67.67	0.31
1	61.04	61.42	0.63
1.1	49.79	55.16	10.79
1.2	41.85	48.91	16.88
1.3	37.83	42.66	12.77
1.4	32.34	36.40	12.58
1.5	24.87	30.15	21.25
1.6	22.37	23.90	6.80
1.7	14.94	17.64	18.07
1.8	14.21	11.39	19.87
1.9	10.02	5.13	48.77
2	9.93	-1.12	111.26

The table shows that the mathematical formulation is reliable only within the wave frequency range below 1. The results indicate that even when the relationship appears nearly linear, deriving a mathematical formulation through linear regression analysis is not reliable enough. For more complex, nonlinear relationships like a polynomial line, the mathematical formulation becomes even more complicated. Consequently, a machine learning model is employed to estimate power production with different parameters.

6.2. Determine Power Relation Using Machine Learning Method

The machine learning analysis begins with data preparation. Multiple results are computed and stored in an xarray.DataFrame within a loop. The data contain parameters with different scales and units, Therefore preprocessing the data is required to scale down the input parameters to a common scale. Standardization is a common preprocessing technique that transforms the data to have a mean of 0 and a standard deviation of 1, shaping them into a standard normal distribution. After setting up the data frame, standardization is applied using the following equation:

$$x_{new} = \frac{(x - \mu)}{\sigma} \tag{6.2}$$

Where x is the original feature value, μ is the mean feature value, σ is the standard deviation of the feature values. Using scaled data instead of the original data is crucial before applying machine learning. One advantage of scaling is that it increases accuracy [47]. Many machine learning algorithms perform better and converge faster when features are on a similar scale. Algorithms can be sensitive to values with large

magnitudes, therefore standardization also helps in faster and more stable convergence. Without scaling, these values may dominate and lead to incorrect results. In this thesis, the Random Forest Regressor and Neural Network are chosen as the algorithms for machine learning. Besides, the input variables of the model are wave frequency, array spacing, and incoming wave direction angle. The computer used for the machine learning process is equipped with an i5-1240P CPU and 16GB of RAM. The performance of the trained models using the above algorithms of the excitation force on each device is evaluated and presented in Figure 6.5, Figure 6.6, Figure 6.7, Figure 6.8. The performance of the model can be evaluated by the coefficient of determination R^2 in the following equation:

$$R^2 = 1 - \frac{\sum_i (x_i - x_{predict})^2}{\sum_i (x_i - \overline{x})^2} \tag{6.3}$$

Where x_i is the actual data, $\overline{x}$ is the mean of the data and $x_{predict}$ is the predicted value. The closer the R^2 value to the one, the more reliable the model is, meaning the predicted load is closer to the actual load. The results show that the model trained by Random Forest Regressor algorithm is more reliable than by Neural Network, as the larger R^2 value indicated.

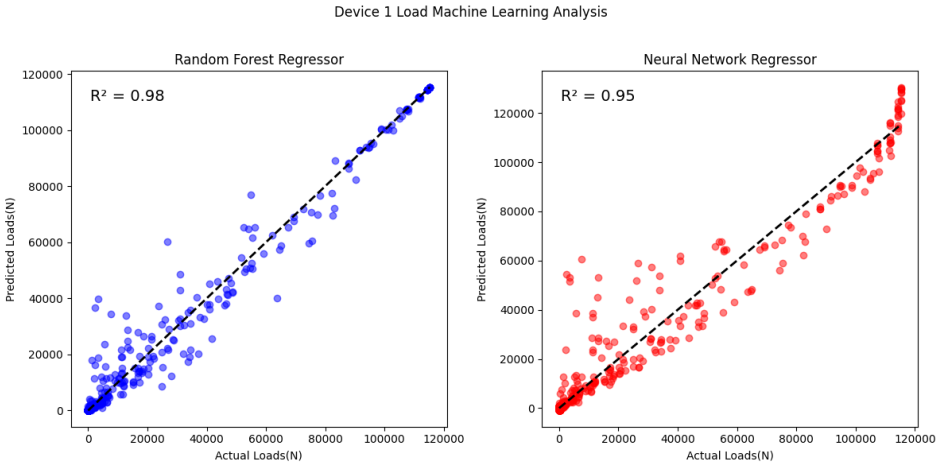

Figure 6.5: Device 1 model performance predicted load

The training of the model for power prediction follows the same steps. However, the significant wave height is now also included in the input variables. The performance of the model is shown in Figure 6.9 and Figure 6.10. The maximum iteration times for Neural Network algorithm were set at 10000, and the total calculation time required is 94 minutes (depending on the computer hardware). However, the resulting predicted power using Neural Network had a bad fit with the actual power. To improve this, The maximum iteration is increased to 100000, and the resulting time required also increases to 237 minutes. However, despite the extended training time, the Neural Network model still did not achieve a better fit with the actual power. To further improve the model, the design is changed from 100 neurons in a single layer to 100 neurons in a single layer and with two layers in total. Unfortunately, a warning message appeared, and the computer crashed. As a result, for the optimization process in the next step, only the Random Forest Regressor model will be used.

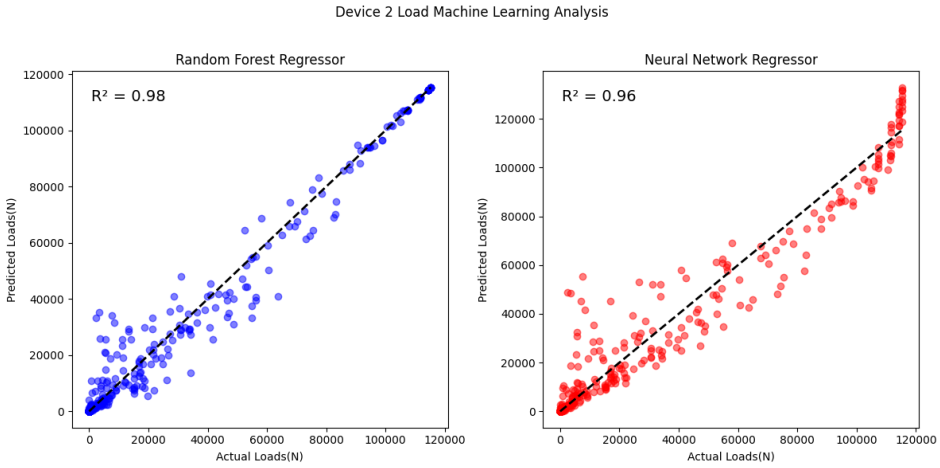

Figure 6.6: Device 2 model performance predicted load

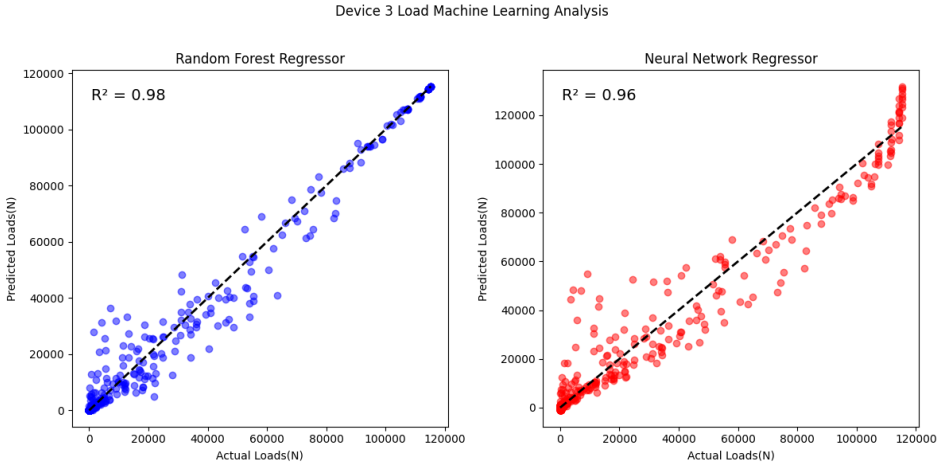

Figure 6.7: Device 3 model performance predicted load

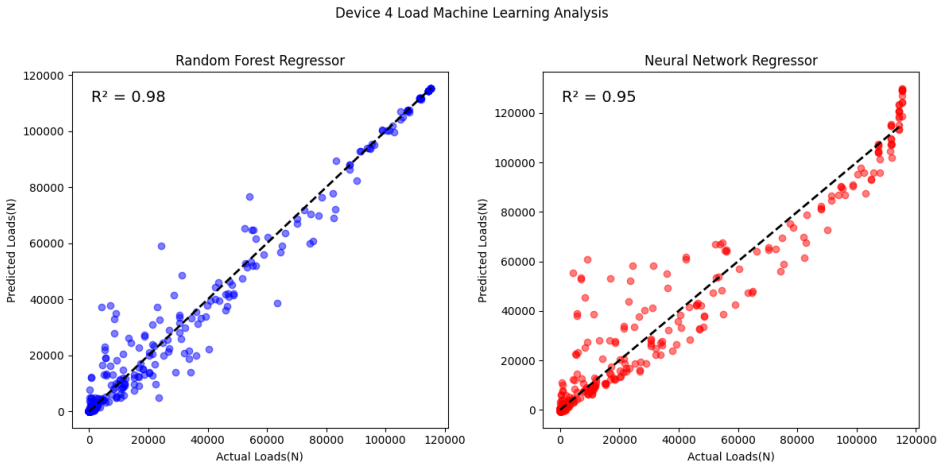

Figure 6.8: Device 4 model performance predicted load

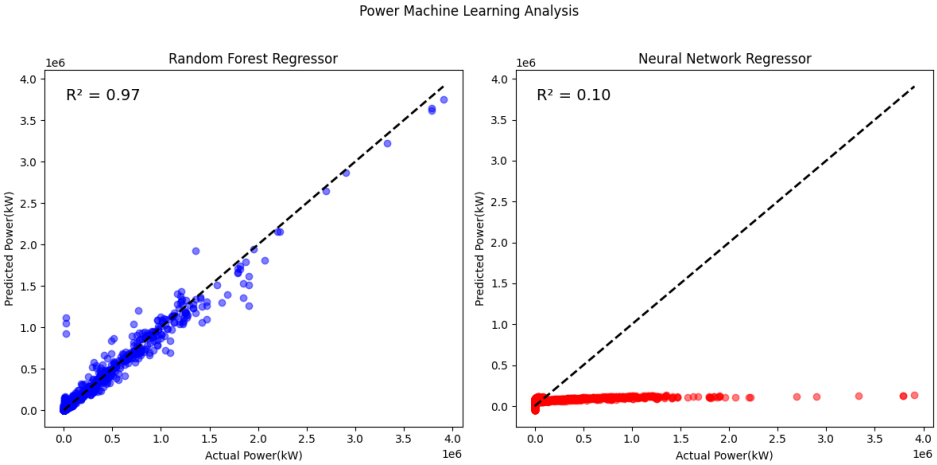

Figure 6.9: Power performance (maximum iteration times =10000)

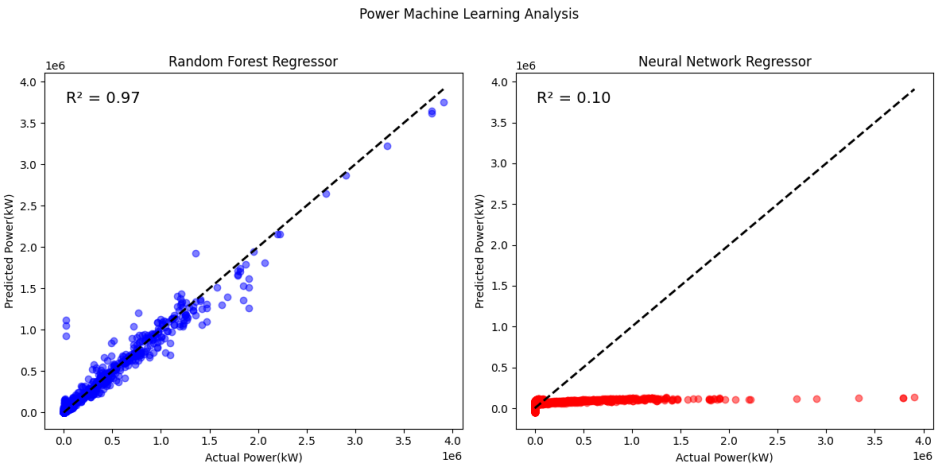

Figure 6.10: Power performance (maximum iteration times =100000)

7

Optimization of Array Desgin

Optimizing the design of an array is essential for maximizing power production in renewable energy systems. Once a power production model is trained, it can predict power output based on various input parameters. This chapter focuses on the optimization process, where the model is used to explore different configurations by inputting randomly generated data. By analyzing the resulting outputs, the optimal array design that yields the maximum power can be identified. This methodology enhances the efficiency of energy systems and contributes to the advancement of sustainable energy solutions.

7.1. Totally Random Data

The most straightforward way to use the model is to find the input factors that result in the maximum predicted power. All the input data, including wave frequency, array spacing, wave direction, and wave height, are generated randomly. By generating a sufficiently large amount of data, the maximum power can be determined by comparing all the data sets. In the analysis, 1,000 sets of data are generated, and the input variables that result in the maximum power are recorded. This process is then repeated six times to check for convergence. The final results are shown in Figure 7.1. Note that the units for the parameters are as follows: frequency is in radians, wave height in meters, wave angle in radians, array spacing in meters, and predicted power in kilowatts. The result indicated that the maximum power output always occurs when the wave frequency is near around 1.27, which is likely the natural frequency value of the wave farm. Additionally, the resulting power output is unrealistically high and is not likely to be observed in the real sea states.

7.2. Random Data in A Given Sea Site

Due to the fact that the maximum power production always occurs when the wave frequency is near the natural frequency of the WECs array, power prediction combined with a wave occurrence matrix was introduced to evaluate the most probable power

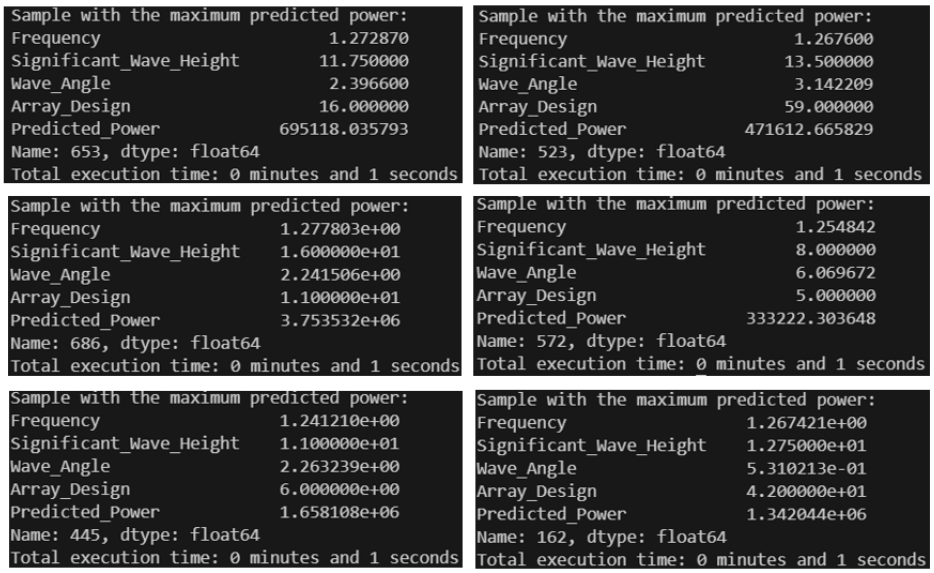

Figure 7.1: Maximum power output and input variables

in a given sea state. A wave occurrence matrix is a diagram showing the probability of occurrence of different wave periods and wave heights at a specific site. By using this matrix along with predicted power at specific periods and wave heights, the most probable power output of the wave farm at this site can be easily estimated. Furthermore, by randomly selecting a large number of wave directions and array spacings and input these data into the model trained in chapter 6, the maximum power and the corresponding wave direction angle and spacing distance can be determined. In this thesis, the wave occurrence matrix from AMETS, Ireland, was used[48]. To evaluate the performance of the array design, the q factor was computed for each analysis. Since the wave frequency and significant wave height are selected based on the diagram, the remaining variables to consider are the wave direction angle and array spacing. By randomly generating 100 sets of these variables and repeating the process six times, the optimal parameters that result in the largest q factor can be determined.

The results show that the wave farm would have the largest q factor at a wave angle of 0.823 to 0.988 radients (around $48°$ to $56°$) and a spacing of 45 meters, with a q factor of 1.06.

Occurrence (%)	Energy period, Te (s)																			
Significant wave height, Hs (m)	4.25	4.75	5.25	5.75	6.25	6.75	7.25	7.75	8.25	8.75	9.25	9.75	10.25	10.75	11.25	11.75	12.25	12.75	13.25	13.75	14.25
14.25	0	0	0	0	0	0	0	0	0	0	0	0	0	0	0	0	0	0	0	0	0
13.75	0	0	0	0	0	0	0	0	0	0	0	0	0	0	0	0	0	0	0	0	0
13.25	0	0	0	0	0	0	0	0	0	0	0	0	0	0	0	0	0	0	0	0	0.01
12.75	0	0	0	0	0	0	0	0	0	0	0	0	0	0	0	0	0	0	0	0.02	0
12.25	0	0	0	0	0	0	0	0	0	0	0	0	0	0	0	0	0	0	0	0	0
11.75	0	0	0	0	0	0	0	0	0	0	0	0	0	0	0	0	0	0	0.01	0	0
11.25	0	0	0	0	0	0	0	0	0	0	0	0	0	0	0	0	0	0.01	0	0	0
10.75	0	0	0	0	0	0	0	0	0	0	0	0	0	0	0	0	0	0.01	0.02	0.01	0
10.25	0	0	0	0	0	0	0	0	0	0	0	0	0	0	0	0	0	0	0	0	0
9.75	0	0	0	0	0	0	0	0	0	0	0	0	0	0	0	0	0.02	0.03	0	0	0
9.25	0	0	0	0	0	0	0	0	0	0	0	0	0	0	0	0	0.03	0.01	0	0	0.02
8.75	0	0	0	0	0	0	0	0	0	0	0	0	0	0	0	0.01	0.02	0	0.01	0.01	0.02
8.25	0	0	0	0	0	0	0	0	0	0	0	0	0	0	0.01	0.02	0	0.02	0.03	0.01	0.01
7.75	0	0	0	0	0	0	0	0	0	0	0	0	0.01	0	0	0.02	0.03	0.05	0.01	0.01	0
7.25	0	0	0	0	0	0	0	0	0	0	0	0	0	0	0.02	0.02	0.05	0.05	0.02	0	0.01
6.75	0	0	0	0	0	0	0	0	0	0	0	0	0	0.02	0.04	0.09	0.09	0.06	0.02	0.01	0.01
6.25	0	0	0	0	0	0	0	0	0	0	0.01	0	0.04	0.09	0.13	0.11	0.09	0.01	0.02	0.02	0.01
5.75	0	0	0	0	0	0	0	0	0	0	0.02	0.02	0.07	0.14	0.14	0.12	0.03	0.02	0.02	0	0
5.25	0	0	0	0	0	0	0	0	0	0.02	0.07	0.14	0.24	0.21	0.14	0.11	0.03	0.02	0	0	0
4.75	0	0	0	0	0	0	0	0	0.06	0.11	0.28	0.34	0.35	0.31	0.22	0.14	0.05	0.02	0	0	0
4.25	0	0	0	0	0	0	0.01	0.08	0.12	0.52	0.6	0.72	0.47	0.27	0.2	0.12	0.08	0	0	0	0
3.75	0	0	0	0	0	0	0.04	0.16	0.5	0.83	0.95	0.86	0.55	0.52	0.37	0.1	0.03	0	0.05	0.01	0.01
3.25	0	0	0	0	0	0.07	0.11	0.51	0.89	1.49	2.06	1.57	1.05	0.68	0.51	0.34	0.1	0.08	0.05	0	0
2.75	0	0	0	0	0.09	0.21	0.74	1.15	2.14	2.61	2.58	1.58	1.15	0.9	0.56	0.39	0.26	0.09	0.1	0.02	0.01
2.25	0	0	0.01	0.02	0.17	0.57	1.71	2.03	2.15	2.42	1.87	1.53	1.18	0.68	0.36	0.21	0.14	0.15	0.13	0.09	0.03
1.75	0	0	0.11	0.67	1.08	1.74	1.93	2.81	3.43	3.71	2.68	1.79	1.15	0.49	0.2	0.17	0.1	0.03	0.02	0	0.01
1.25	0	0.02	0.46	1.34	0.92	1.5	2.18	2.38	3.1	2.24	2.28	1.74	1.02	0.55	0.2	0.03	0.05	0.05	0	0	0
0.75	0	0.09	0.14	0.55	0.3	0.71	0.95	0.79	0.49	0.33	0.4	0.14	0.06	0.03	0.02	0	0.01	0	0	0	0
0.25	0	0	0	0	0	0	0	0	0.01	0	0	0	0	0	0	0	0	0	0	0	0

Figure 7.2: Wave scatter plot showing the wave occurrence for the AMETS site, Ireland[48]

```
Wave_Direction [rad]      0.858953
Array_Spacing [m]        46.000000
Total_Power [kW]         52.034097
q_factor [-]              1.064791
Name: 1394, dtype: float64
Total execution time: 0 minutes and 40 seconds
```

```
Wave_Direction [rad]      0.866258
Array_Spacing [m]        46.000000
Total_Power [kW]         52.034097
q_factor [-]              1.064791
Name: 1491, dtype: float64
Total execution time: 0 minutes and 39 seconds
```

```
Wave_Direction [rad]      0.822645
Array_Spacing [m]        45.000000
Total_Power [kW]         52.034097
q_factor [-]              1.064791
Name: 889, dtype: float64
Total execution time: 0 minutes and 39 seconds
```

```
Wave_Direction [rad]      0.917346
Array_Spacing [m]        45.000000
Total_Power [kW]         52.034097
q_factor [-]              1.064791
Name: 1494, dtype: float64
Total execution time: 0 minutes and 38 seconds
```

```
Wave_Direction [rad]      0.843017
Array_Spacing [m]        46.000000
Total_Power [kW]         52.034097
q_factor [-]              1.064791
Name: 1493, dtype: float64
Total execution time: 0 minutes and 40 seconds
```

```
Wave_Direction [rad]      0.987846
Array_Spacing [m]        45.000000
Total_Power [kW]         52.034097
q_factor [-]              1.064791
Name: 1597, dtype: float64
Total execution time: 0 minutes and 38 seconds
```

Figure 7.3: Optimal q factor and other design parameters

8

Conclusion and Recommendations

8.1. Conclusion

The objectives that the thesis is going to complete are:

1. Perform hydrodynamic analysis using frequency domain BEM software Capytaine of a single device as well as the wave farm consisting of 4 devices arranged in a square configuration.
2. Setting up the relation of the various parameters with the excitation force on each device and the total power output
3. Perform optimization using the previously trained model to find the optimal configuration that results in the highest probable power output for a given site.

Previous research has shown that optimization studies often require a lot of time and high computility. Consequently, the goal of this research is to develop a method (either by establishing a mathematical relationship or training a machine learning model) that can reduce the time required during the design phase. Finally, this approach can significantly shorten the estimation time and accelerate the design process.

The hydrodynamic analysis was performed on a cylindrical point absorber. By calculating its hydrodynamic characteristics using Capytaine, the power output in regular waves was determined, and the result show that the maximum power occurs at the natural frequency of the single device. To analyze the wave field within the wave farm, additional devices were added to form a WEC array.

The relationship of the design parameters and the power output as well as the excitation force was initially derived using linear regression. Despite the straightforward calculation process, the mathematical function of the power output did not fit the original data well. Therefore, a machine learning approach was used to provide a more accurate solution for determining this relationship. The Random Forest Regressor and Neural Network algorithms were used for the analysis. While both algorithms provided a good fit for the excitation force model, the Neural Network model did not perform well for predicting power output compared to the Random Forest Regressor.

After training the model, it is possible to predict the performance of a wave farm consisting of 4 buoys in a given sea state. Only the model trained in Random Forest Regressor was used due to the better performance. By the usage of wave occurrence diagram the power output in a site can be easily estimated. The optimal q factor is achieved when wave direction is between 48 to 56 degree and array spacing is 45 meters.

8.2. Recommendations

In order to improve future work related to WEC array design, several recommendations can be made.

The optimization method used in this thesis relies on estimated power output from a machine learning-trained model. While the randomly selected samples help ensure that the optimal q factor is identified, the results are based on a human-designed model, which may not perfectly align with the results from direct calculations. Therefore, comparing the Monte Carlo Method or Genetic Algorithm with the optimization results from this thesis would provide valuable support and validation.

Additionally, the number of panels used in the WEC model in this thesis is set to the default value from the CAD software. Conducting a convergence study on the panel numbers could help identify the optimal number of panels, enabling more efficient analysis in further hydrodynamic analysis.

Furthermore, the PTO damping coefficient in the thesis is selected based on the natural frequency of the floating device, and the machine learning model is trained based on this feature to predict power performance at any sea site. However, the optimal PTO damping coefficient varies depending on the sea site, which limits the ability to train a model that applies to all locations. Despite the consistency of the optimal power damping coefficient under different wave periods shown in Figure A.13, additional steps can be taken to further improve the model. One approach is to train multiple machine learning models, each under different PTO damping coefficients. When a test sea site is selected, these models can be used to predict the power performance and identify the best optimal PTO coefficient that maximizes the q factor in this sea site.

References

[1] S. H. Salter M.A. “World progress in wave energy—1988”. In: *International Journal of Ambient Energy* (2011), pp. 3–24.

[2] António F. de O. Falcão. “Wave energy utilization: A review of the technologies”. In: *Renewable and Sustainable Energy Reviews* (2010), pp. 899–918.

[3] *European Commission*. https://oceans-and-fisheries.ec.europa.eu/news/wavefarm-unleashes-wave-energy-sustainable-future-2024-01-31_en. 2024.

[4] Iván A. Hernández-Robles et al. “Wave power assessment for electricity generation with powerbouy system by wave motion emulation modelling”. In: *Sustainable Energy Technologies and Assessments* 43 (2021).

[5] Chong-wei Zheng et al. “Assessing the China Sea wind energy and wave energy resources from 1988 to 2009”. In: *Ocean Engineering* (2013), pp. 39–48.

[6] Alain Clément et al. “Wave energy in Europe: current status and perspectives”. In: *Renewable and Sustainable Energy Reviews* (2002), pp. 405–431.

[7] Marcus Lehmann et al. “Ocean wave energy in the United States: Current status and future perspectives”. In: *Renewable and Sustainable Energy Reviews* (2017), pp. 1300–1313.

[8] Yongxing Zhang et al. “Ocean wave energy converters: Technical principle, device realization, and performance evaluation”. In: *Renewable and Sustainable Energy Reviews* 141 (2021).

[9] António F.O. Falcão et al. “Oscillating-water-column wave energy converters and air turbines: A review”. In: *Renewable Energy* (2016), pp. 1391–1424.

[10] T. V. Heath. “A Review of Oscillating Water Columns”. In: *Philosophical Transactions of the Royal Society A: Mathematical, Physical and Engineering Sciences* (2012).

[11] D. V. Evans. “The Oscillating Water Column Wave-energy Device”. In: *IMA Journal of Applied Mathematics* (1978), pp. 423–433.

[12] Matthieu Ancellin. *Run hydrostatics for multiple bodies 188*. https://github.com/capytaine/capytaine/issues/188. 2022.

[13] Bret Bosma et al. “Wave energy converter modeling in the frequency domain: A design guide”. In: *2012 IEEE Energy Conversion Congress and Exposition (ECCE)* (2012).

[14] J.N. NEWMAN. “Algorithms for the free-surface Green function”. In: *Journal of Engineering Mathematics volume* (1985), pp. 57–67.

[15] Matt Folley. *Numerical Modelling of Wave Energy Converters*. Elsevier, 2016. ISBN: 978-0-12-803210-7.

[16] J.N. NEWMAN. *Marine Hydrodynamics*. The MIT Press, 1977. ISBN: 9780262534826.

[17] J.N. NEWMAN. “The approximation of free-surface Green functions”. In: *Wave asymptotics* (1992), pp. 107–135.

[18] Ryan G. Coe et al. “Nonlinear time-domain performance model for a wave energy converter in three dimensions”. In: *2014 Oceans - St. John’s* (2014).

[19] A. Babarit and A.H. Clément. “Optimal latching control of a wave energy device in regular and irregular waves”. In: *Applied Ocean Research* (2006).

[20] W. E. Cummins. *The Impulse Response Function and Ship Motions*. Department of the Navy, David Taylor Model Basin, 1962. URL: `https://dome.mit.edu/bitstream/handle/1721.3/49049/DTMB_1962_1661.pdf`.

[21] W.E. Cummins. *The Impulse Response Function and Ship Motions*. Defense Technical Information Center, 1962, pp. 378–389.

[22] Ebrahim Hamid Hussein Al-Qadami et al. “Numerical modelling of flow characteristics over sharp crested triangular hump”. In: *Results in Engineering* (2019).

[23] Mohammad Jafari et al. “Numerical simulation of a novel ocean wave energy converter”. In: *Energy Procedia* (2018), pp. 474–481.

[24] Yi-Hsiang Yu et al. *WEC-Sim Webinar*. `https://wec-sim.github.io/WEC-Sim/dev/_static/downloads/WEC-Sim_Webinar2.pdf`. 2017.

[25] B. Borgarino et al. “Impact of wave interactions effects on energy absorption in large arrays of wave energy converters”. In: *Ocean Engineering* (2011), pp. 79–88.

[26] Bo Yang et al. “Wave energy converter array layout optimization: A critical and comprehensive overview”. In: *Renewable and Sustainable Energy Reviews* (2022).

[27] Seyedali Mirjalili. *Evolutionary Algorithms and Neural Networks*. SPRINGER LINK, 2018. ISBN: 978-3-319-93024-4.

[28] Batta Mahesh. “Machine Learning Algorithms - A Review”. In: *International Journal of Science and Research* (2018).

[29] Gérard Biau and Erwan Scornet. “A random forest guided tour”. In: *TEST* (2016).

[30] N. Krishna Kumar et al. “Ocean wave characteristics prediction and its load estimation on marine structures: A transfer learning approach”. In: *Marine Structures* (2018), pp. 205–219.

[31] Zheng Wu et al. “Load optimization control of SJTU-WEC based on machine learning”. In: *Ocean Engineering* (2022).

[32] Shuo Shi et al. “Wave Excitation Force Estimation and Forecasting for WEC Power Conversion Maximisation”. In: *International Conference on Advanced Intelligent Mechatronics* (2022).

[33] Malin Göteman. “Wave energy parks with point-absorbers of different dimensions”. In: *Journal of Fluids and Structures* (2017), pp. 142–157.

[34] Silvia Bozzi et al. “Wave energy farm design in real wave climates: the Italian offshore”. In: *Energy* (2017), pp. 378–389.

[35] A.Jabrali et al. “WEC Parameters Optimization by Genetic Algorithm Method”. In: *VII International Conference on Computational Methods in Marine Engineering*. 2017.

[36] Marianna Giassi et al. “Economical layout optimization of wave energy parks clustered in electrical subsystems”. In: *Applied Ocean Research* 102274 (2020).

[37] Chris Sharp and Bryony DuPont. “Wave Energy Converter Array Optimization: A Review of Current Work and Preliminary Results of a Genetic Algorithm Approach Introducing Cost Factors”. In: *ASME 2015 International Design Engineering Technical Conferences and Computers and Information in Engineering Conference*. Boston, Massachusetts, USA: ASME, 2016.

[38] Mehdi Neshat et al. “A hybrid cooperative co-evolution algorithm framework for optimising power take off and placements of wave energy converters”. In: *Information Science* (2020), pp. 218–244.

[39] Alejandro López-Ruiz et al. “Towards an optimum design of wave energy converter arrays through an integrated approach of life cycle performance and operational capacity”. In: *Applied Energy* (2018), pp. 20–32.

[40] E. Faraggiana et al. “Design of an optimization scheme for the WaveSub array”. In: *RENEW 2018*. 2018.

[41] Alberto Montanari. *Mechanics of sea waves*. `https://www.albertomontanari.it/node/123`. 2017.

[42] Jørgen Hals Todalshaug et al. “Optimum Reactive Control and Control by Latching of a Wave-Absorbing Semisubmerged Heaving Sphere”. In: *ASME 2002 21st International Conference on Offshore Mechanics and Arctic Engineering*. 2002.

[43] Mat´ıas Alday G. et al. “Analysis of the North Atlantic offshore energy flux from different reanalysis and hindcasts”. In: *PROCEEDINGS OF THE 15TH EUROPEAN WAVE AND TIDAL ENERGY CONFERENCE*. 2023.

[44] Edgard Malta et al. “Damping Coefficient Analyses for Floating Offshore Structures”. In: *29th International Conference on Ocean, Offshore and Arctic Engineering (OMAE2010)*. 2010.

[45] *Rhino 3D*. `https://www.rhino3d.com/`. 2024.

[46] *Matlab Help Center*. `https://nl.mathworks.com/help/matlab/ref/polyfit.html`. 2024.

[47] Gozde Karatas. “The Effects of Normalization and Standardization an Internet of Things Attack Detection”. In: *European Journal of Science and Technology* (2021).

[48] James Prendergast et al. “A Study on the Effects of Wave Spectra on Wave Energy Conversions”. In: *JOURNAL OF OCEANIC ENGINEERING* (2018).

A

Supplement Information

A.1. Linear Relation Equations of Excitation Force

- Device 1 angle=0°

$$F_{ex}(x, y) = (0.041 \cdot x - 64.166) \cdot y + (-0.084 \cdot x + 127.31) \tag{A.1}$$

- Device 1 angle=45°

$$F_{ex}(x, y) = (0.072 \cdot x - 65.041) \cdot y + (-0.134 \cdot x + 128.891) \tag{A.2}$$

- Device 1 angle=90°

$$F_{ex}(x, y) = (0.041 \cdot x - 64.178) \cdot y + (-0.085 \cdot x + 127.346) \tag{A.3}$$

- Device 2 angle=0°

$$F_{ex}(x, y) = (0.041 \cdot x - 64.178) \cdot y + (-0.085 \cdot x + 127.346) \tag{A.4}$$

- Device 2 angle=45°

$$F_{ex}(x, y) = (0.04 \cdot x - 63.895) \cdot y + (-0.052 \cdot x + 125.624) \tag{A.5}$$

- Device 2 angle=90°

$$F_{ex}(x, y) = (-0.026 \cdot x - 61.329) \cdot y + (0.05 \cdot x + 121.819) \tag{A.6}$$

- Device 3 angle=0°

$$F_{ex}(x, y) = (-0.023 \cdot x - 61.41) \cdot y + (0.048 \cdot x + 121.86) \tag{A.7}$$

- Device 3 angle=45°

$$F_{ex}(x, y) = (0.042 \cdot x - 63.946) \cdot y + (-0.052 \cdot x + 125.64) \tag{A.8}$$

- Device 3 angle=$90°$

$$F_{ex}(x, y) = (0.041 \cdot x - 64.166) \cdot y + (-0.084 \cdot x + 127.31) \tag{A.9}$$

- Device 4 angle=$0°$

$$F_{ex}(x, y) = (-0.026 \cdot x - 61.33) \cdot y + (0.05 \cdot x + 121.82) \tag{A.10}$$

- Device 4 angle=$45°$

$$F_{ex}(x, y) = (0.005 \cdot x - 62.044) \cdot y + (0.041 \cdot x + 121.338) \tag{A.11}$$

- Device 4 angle=$90°$

$$F_{ex}(x, y) = (-0.023 \cdot x - 61.41) \cdot y + (0.048 \cdot x + 121.86) \tag{A.12}$$

A.2. Figures

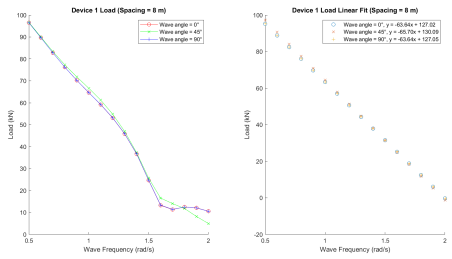

(a) Device 1

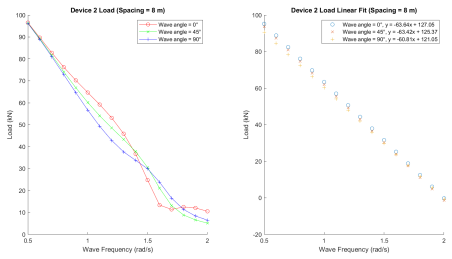

(b) Device 2

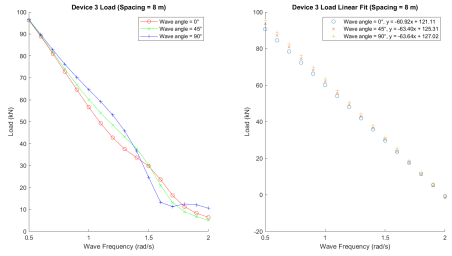

(c) Device 3

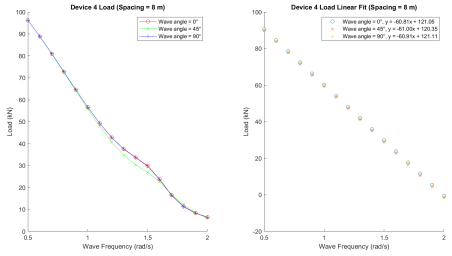

(d) Device 4

Figure A.1: Excitation Force at spacing = 8 meters

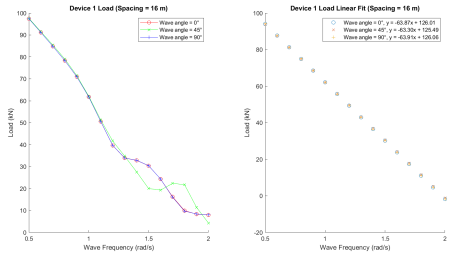

(a) Device 1

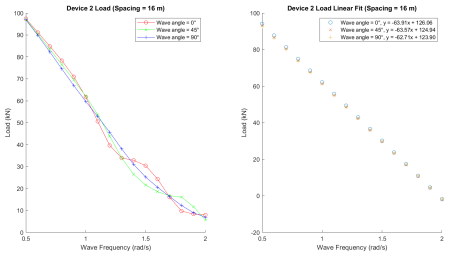

(b) Device 2

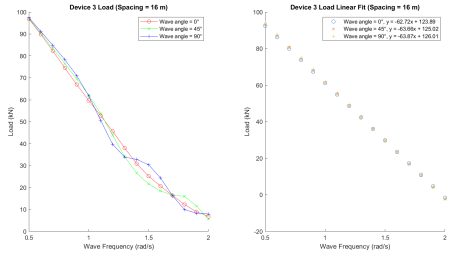

(c) Device 3

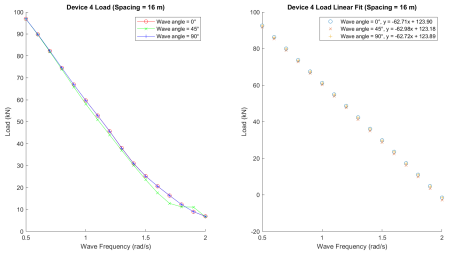

(d) Device 4

Figure A.2: Excitation Force at spacing = 16 meters

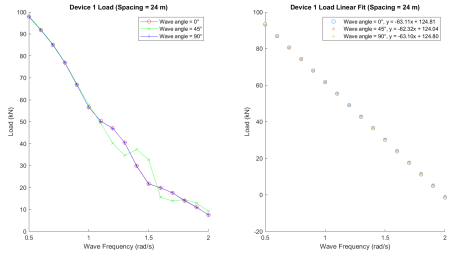

(a) Device 1

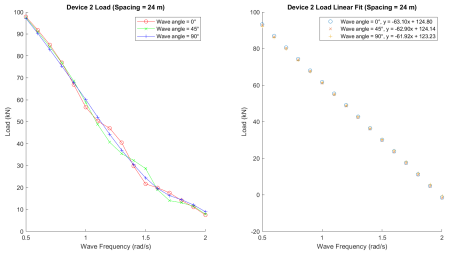

(b) Device 2

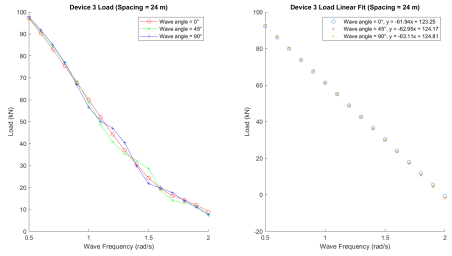

(c) Device 3

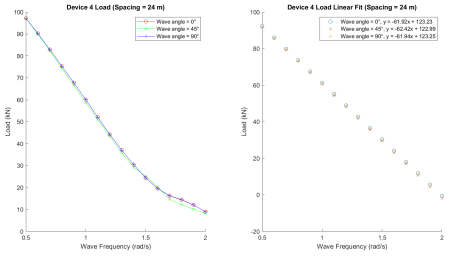

(d) Device 4

Figure A.3: Excitation Force at spacing = 24 meters

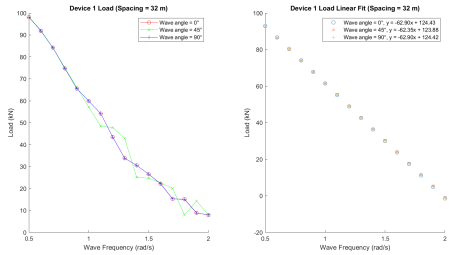

(a) Device 1

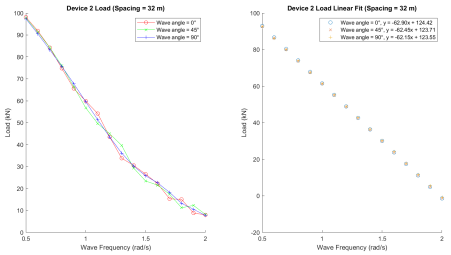

(b) Device 2

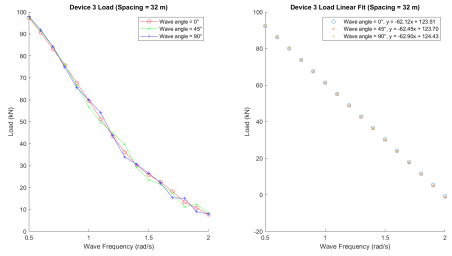

(c) Device 3

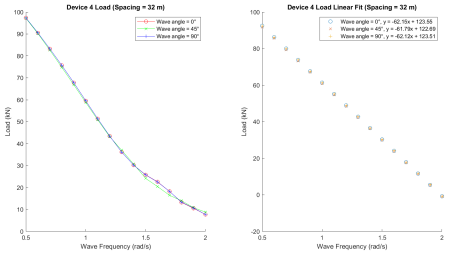

(d) Device 4

Figure A.4: Excitation Force at spacing = 32 meters

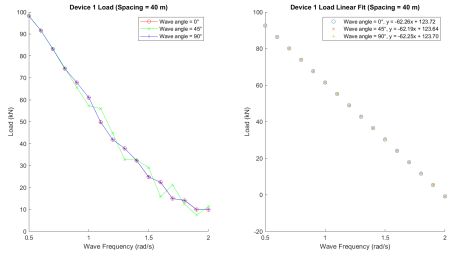

(a) Device 1

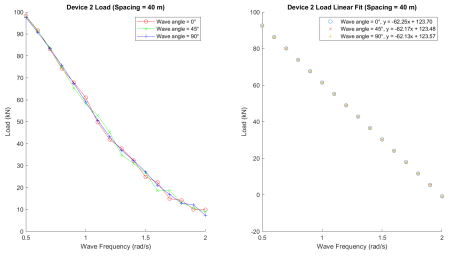

(b) Device 2

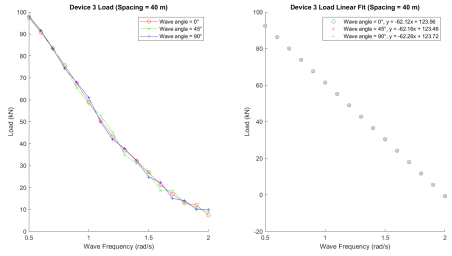

(c) Device 3

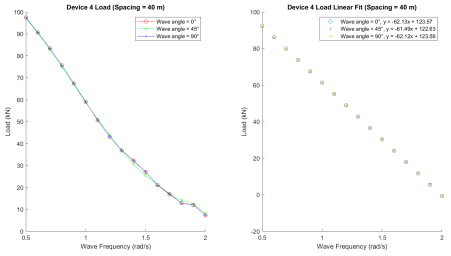

(d) Device 4

Figure A.5: Excitation Force at spacing = 40 meters

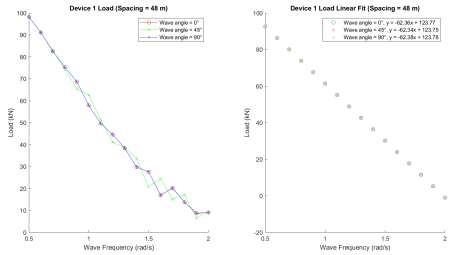

(a) Device 1

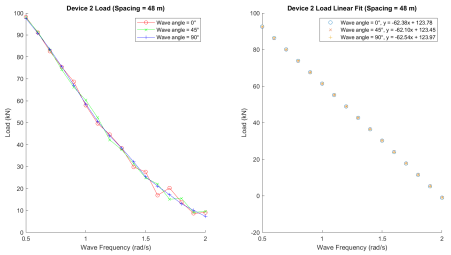

(b) Device 2

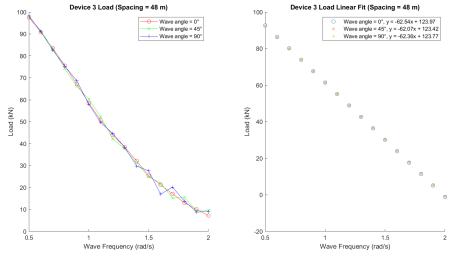

(c) Device 3

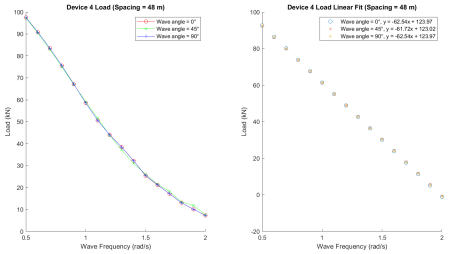

(d) Device 4

Figure A.6: Excitation Force at spacing = 48 meters

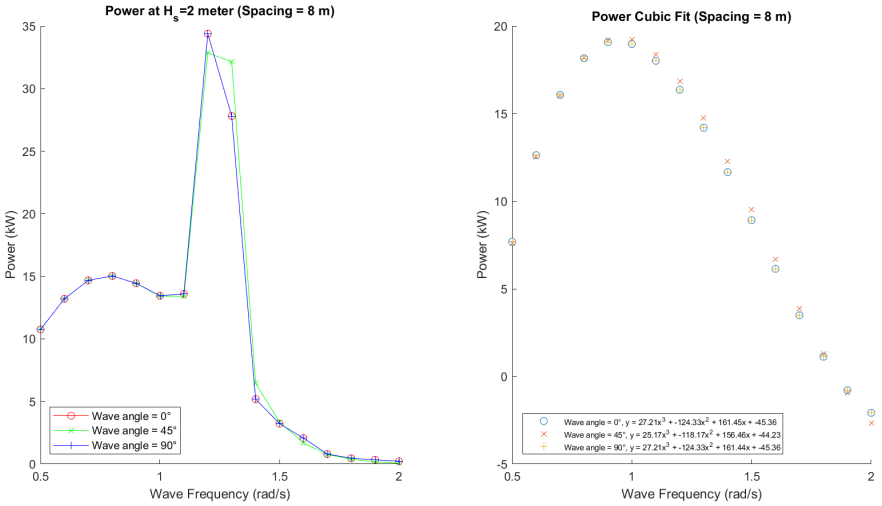

Figure A.7: Power analysis for spacing = 8 meters

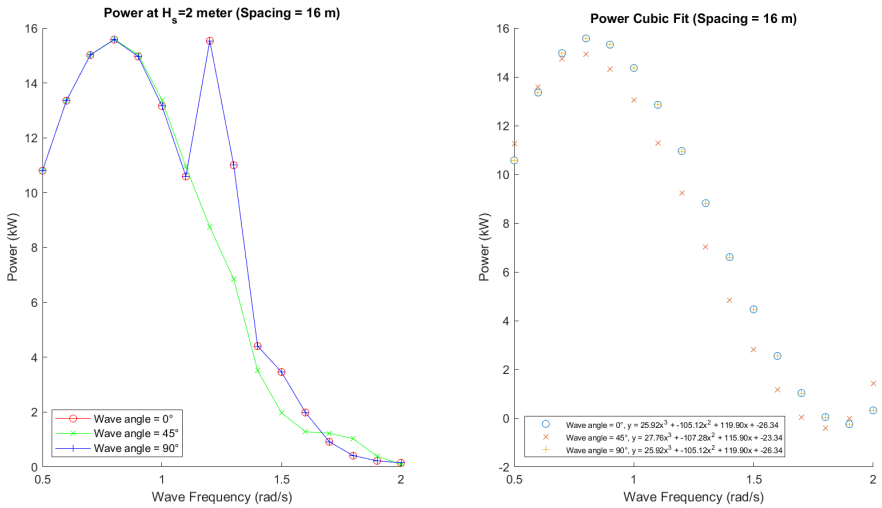

Figure A.8: Power analysis for spacing = 16 meters

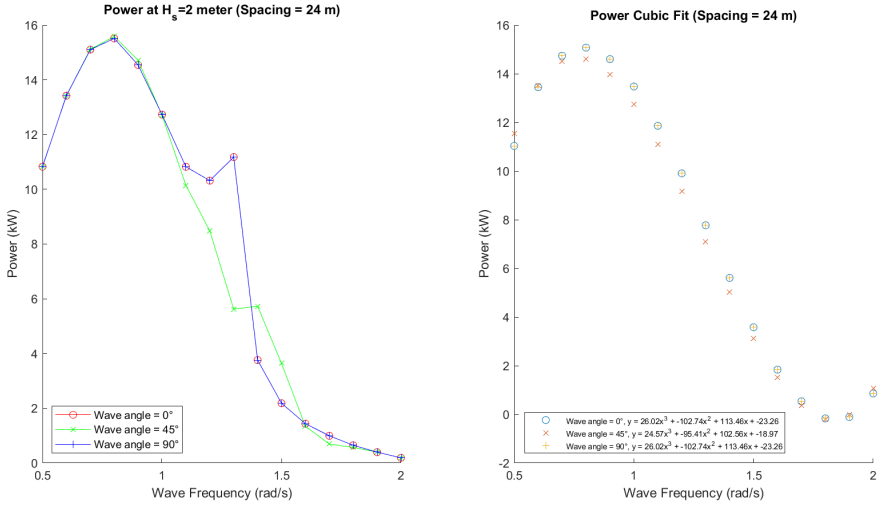

Figure A.9: Power analysis for spacing = 24 meters

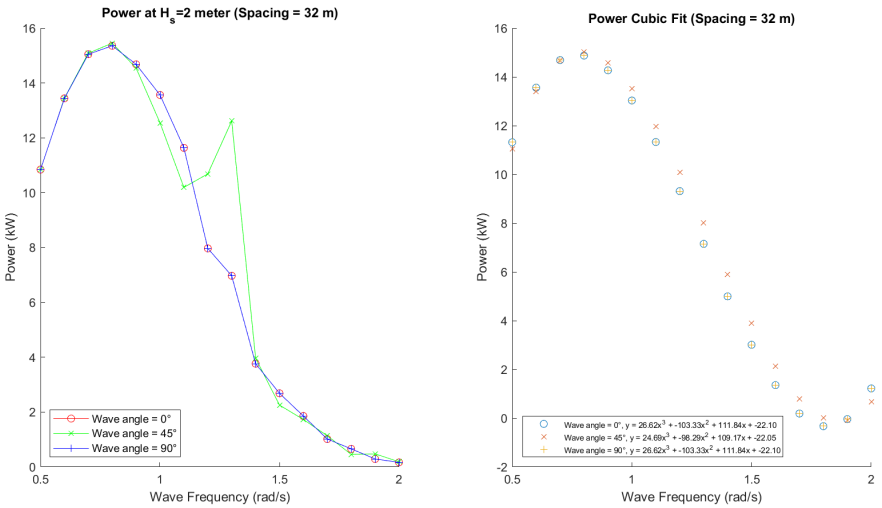

Figure A.10: Power analysis for spacing = 32 meters

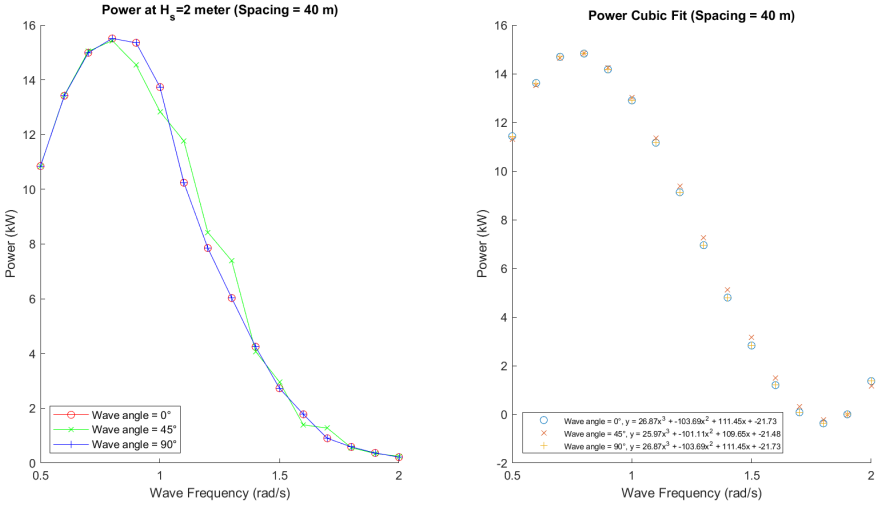

Figure A.11: Power analysis for spacing = 40 meters

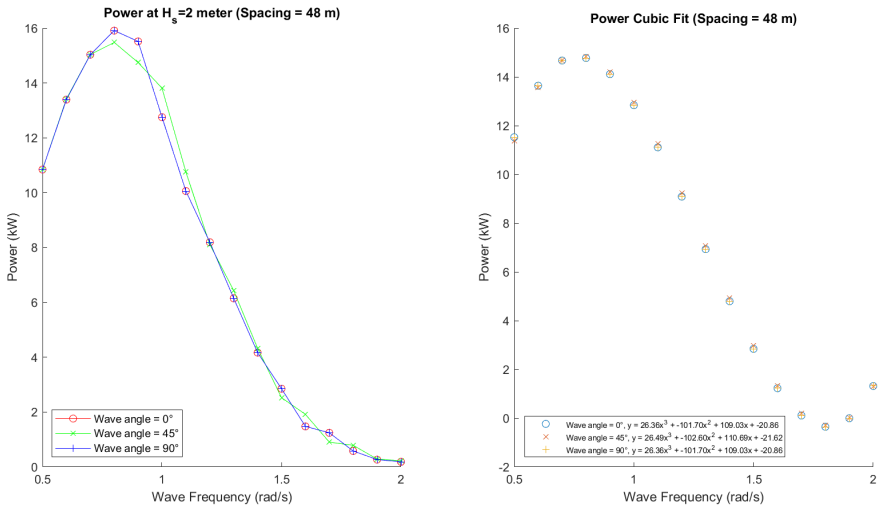

Figure A.12: Power analysis for spacing = 48 meters

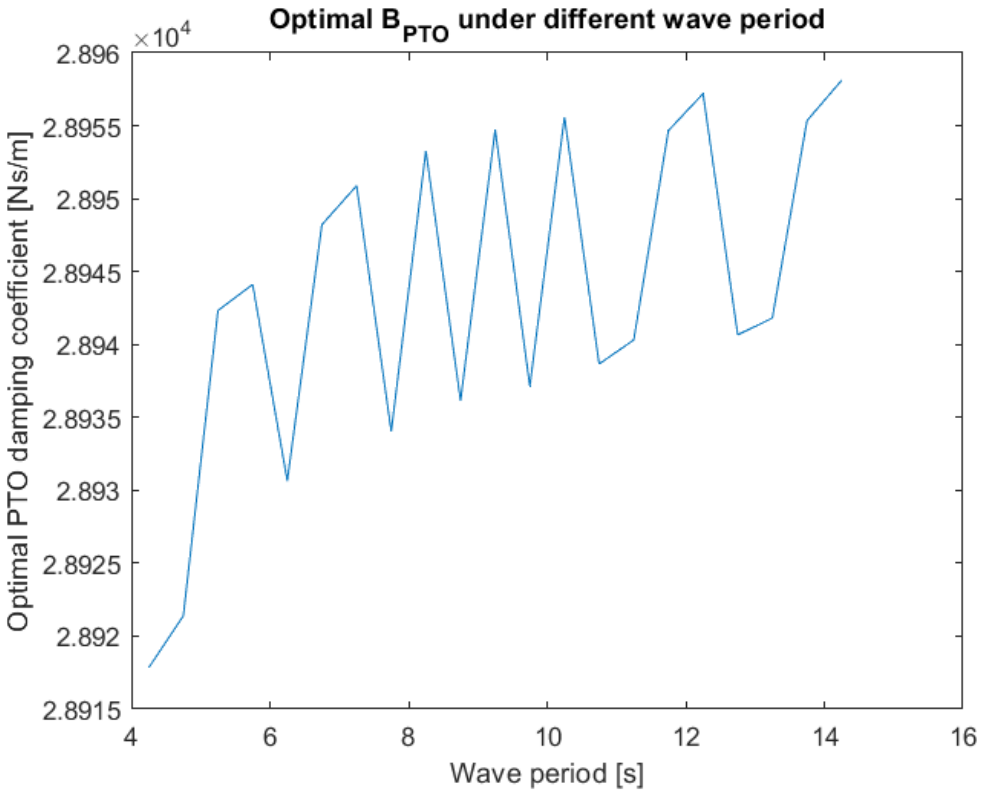

Figure A.13: Optimal power damping coefficient variation under different wave periods